Control of Hematopoietic Stem Cell Function Through Epigenetic Regulation of Energy Metabolism and Genome Integrity

Zhenhua Yang[1], Kushani Shah[1], Alireza Khodadadi-Jamayran[1], and Hao Jiang[1, 2]

[1]Department of Biochemistry and Molecular Genetics, University of Alabama at Birmingham School of Medicine

[2]Department of Biochemistry and Molecular Genetics, University of Virginia School of Medicine

Correspondence (Lead Contact):

Hao Jiang
Department of Biochemistry and Molecular Genetics
University of Virginia School of Medicine
PO Box 800733
1340 JPA, Pinn Hall Room 6017
Charlottesville, VA 22908
Phone: (434) 924-2112
Email: hj8d@virginia.edu

The authors have declared that no conflict of interest exists.

Keywords:
hematopoietic stem cells, Dpy30, H3K4 methylation, epigenetic regulation, energy, metabolism, DNA damage response

ABSTRACT

It remains largely unclear how stem cells regulate bioenergetics and genome integrity to ensure tissue homeostasis. Here, our integrative gene analyses suggest metabolic and genotoxic stresses may underlie the common functional defects of both fetal and adult hematopoietic stem cells (HSCs) upon loss of Dpy30, an epigenetic modulator that facilitates H3K4 methylation. Dpy30 directly regulates expression of several key glycolytic genes, and its loss in HSCs critically impaired energy metabolism, including both glycolytic and mitochondrial pathways. We also found significant increase in DNA breaks as a result of impaired DNA repair upon Dpy30 loss, and inhibition of DNA damage response partially rescued clonogenicity of the Dpy30-deficient HSCs. Moreover, CDK inhibitor p21 was upregulated in Dpy30-deficient HSCs, and *p21* deletion alleviated their functional defect. These results demonstrate that epigenetic mechanisms by H3K4 methylation play a crucial role in HSC function through control of energy metabolism and protecting genome integrity.

INTRODUCTION

The mission of the somatic stem cells is to maintain the tissue homeostasis throughout the lifespan of an organism. To accomplish this mission, stem cells have two defining properties, self-renewal to replenish themselves, and differentiation to give arise to cells of all lineages in the specific tissue. Adult tissue stem cells, including hematopoietic stem and progenitor cells (HSCs and HPCs, or HSPCs), usually remain in the quiescent state with limited cell divisions, but can enter rapid proliferation upon activation (Kondo et al., 2003).

As one of the most fundamental processes of all lives, metabolism profoundly influences the fate determination of stem and progenitor cells (Ito and Suda, 2014). Quiescent HSCs have relatively inactive mitochondria and mainly rely on glycolysis, but rapidly switch to mitochondrial oxidative phosphorylation as the major energy supply when they undergo activation and differentiation (Folmes et al., 2012; Ito and Suda, 2014). How HSCs regulate their metabolism to ensure correct decision making of cell fate is incompletely understood. As the rate of numerous reactions involved in metabolic pathways are catalyzed by enzymes, metabolism is controlled by the expression level and activities of these metabolic enzymes. Therefore, regulatory mechanisms in gene expression, including epigenetic mechanisms can play an important role in stem cell fate determination through impinging on the metabolic pathways in the cell. Histone H3K4 methylation is one of the most prominent epigenetic marks associated with active gene expression (Martin and Zhang, 2005; Shilatifard, 2008), but its role in regulation of metabolism, especially in stem cell settings, remains unclear.

Maintaining the stability of the genetic material is another fundamental cellular process critical for any cells, and is particularly crucial for stem cells to ensure the propagation of correct genetic information throughout the daughter cells in the tissue for the benefit of the whole organism (Blanpain et al., 2011). Following the detection of DNA lesions, the intricate network of DNA damage response (DDR) orchestrates a signal transduction pathway that activates multiple layers of decisions, including cell cycle arrest, apoptosis, senescence, as well as DNA repair (Ciccia and Elledge, 2010). The importance of DDR in HSC function has been well demonstrated by sever HSC defects in mice deficient of active components in either recognition (Ito et al., 2004) or repair (Nijnik et al., 2007; Rossi et al., 2007) of DNA lesions in the DDR pathways. As DDR occurs in the context of chromatin, it is thus governed by epigenetic mechanisms regulating chromatin structure and accessibility (Lukas et al., 2011; Price and D'Andrea, 2013). In addition to the well-established association with active gene expression, a role of H3K4 methylation in regulating genome stability is also gradually emerging (Burman et al., 2015; Faucher and

Wellinger, 2010; Herbette et al., 2017; Higgs et al., 2018), but how this epigenetic modification regulates stem cell function through its role in DDR is much less understood.

The most notable H3K4 methylation enzymes in mammals are the Set1/Mll complexes (Shilatifard, 2008), which comprise one of six different catalytic subunits and several shared core subunits including Dpy30. We have previously shown that Dpy30 directly facilitates genome-wide H3K4 methylation (Jiang et al., 2011) and plays important roles in the fate transition between pluripotent and differentiated states (Jiang et al., 2011; Yang et al., 2015). We have further shown a crucial role of Dpy30 in HSPCs and animal hematopoiesis (Yang et al., 2014). Ablation of *Dpy30* in the hematopoietic system of the adult mouse bone marrow (BM) leads to loss of global H3K4 methylation, and disables differentiation and long-term maintenance of adult HSCs (Yang et al., 2016). This is shown in part by the striking accumulation of phenotypic HSCs and early HPCs at the expense of more downstream hematopoietic cells after *Dpy30* ablation in BM (Yang et al., 2016). Moreover, Dpy30-deficient adult HSCs contribute poorly to all hematopoietic cell populations in the later stage after transplant. The normal transition of gene program between cell populations is also disrupted, and multiple genes important for HSC maintenance and differentiation are dysregulated following Dpy30 loss (Yang et al., 2016). However, it is unclear what pathways are fundamentally important for Dpy30's role in HSPC fate determination.

It is conceivable that an epigenetic modulator, with its numerous genomic targets, can regulate many different pathways in different biological systems. We reason that pathways fundamentally important for the activity of the modulator are likely to be conserved in different systems. As fetal and adult HSCs differ in many aspects including cell cycle regulation, self-renewal potential, surface marker expression and reconstitution ability (Orkin and Zon, 2008), the function of *Dpy30* and H3K4 methylation in prenatal HSCs is still unknown. In this work, we first revealed a similar requirement of Dpy30 in the activation and long-term maintenance of fetal HSPCs as compared to the adult HSPCs. Our dissection of targets shared in these two systems allowed us to identify energy metabolism and DDR as fundamentally important mediators of the H3K4 methylation pathway in hematopoiesis, as further supported by our rescue assays.

RESULTS

Dpy30 deficiency in fetal liver results in anemia and accumulation of early HSPCs

We previously generated a *Dpy30* conditional knockout (KO) mouse model where the Floxed (*F*) allele of *Dpy30* is converted to a null allele upon Cre activity (Yang et al., 2016). Based on this and the *Vav-Cre* (Stadtfeld and Graf, 2005) mouse models, here we generated *Dpy30*$^{F/+}$, *Dpy30*$^{F/-}$, *Vav-Cre; Dpy30*$^{F/+}$,

and *Vav-Cre; Dpy30*$^{F/-}$ fetuses in the same litters. The *Vav-Cre; Dpy30*$^{F/-}$ fetuses developed normally until E13.5 (data not shown), a time when Vav-Cre-mediated excision in HSCs becomes fully penetrant (Gan et al., 2010). The *Vav-Cre; Dpy30*$^{F/-}$ fetuses were anemic at E14.5 and anemia became more severe at E15.5 (**Figure 1A**). No difference was observed among the *Dpy30*$^{F/+}$, *Dpy30*$^{F/-}$, and *Vav-Cre; Dpy30*$^{F/+}$ fetuses. We confirmed *Dpy30* excision (**Figure S1A**) and dramatic reduction of *Dpy30* mRNA (**Figure S1B**) and protein (**Figure 1B**) in the *Vav-Cre; Dpy30*$^{F/-}$ fetal livers (FLs). Dpy30 loss also resulted in marked reduction in H3K4 tri-methylation (H3K4me3) and mild reduction in H3K4 mono- and di-methylation (**Figure 1B**).

While the number of total mononuclear FL cells was not affected, we consistently detected a striking accumulation (**Figures 1C, S1C, and S1D**), in absolute number and frequency, of lineage negative (Lin$^-$) cells and early HSPCs including LT-HSCs, ST-HSCs, Restricted Lineage Progenitors (RLPs) (Kiel et al., 2005), and Lin$^-$ Sca1$^+$c-Kit$^+$ (LSK) cells (see **Table S1** for cell surface markers) in the *Vav-Cre; Dpy30*$^{F/-}$ FLs. Conversely, the frequency of lineage positive (Lin$^+$) cells was decreased (**Figure S1C**). Dpy30 loss in FLs did not affect the proliferation of multipotent stem cells (LT-HSCs and ST-HSCs), but significantly reduced the proliferation of oligopotent progenitors (RLP) and Lin$^+$ cells (**Figure S1E, left**). Apoptosis was unaffected in all FL cell fractions upon Dpy30 loss (**Figure S1E, right**).

Dpy30-deficient fetal liver HSCs are defective in differentiation and long-term maintenance

Compared to the *Vav-Cre*; *Dpy30*$^{F/+}$ FLs, the *Vav-Cre*; *Dpy30*$^{F/-}$ FLs cells were severely defective in forming any types of colonies in methylcellulose (**Figure S1F**). In competitive transplantation assays (**Figure S1G**), the *Vav-Cre*; *Dpy30*$^{F/-}$ FLs were severely defective in reconstituting multiple peripheral blood (PB) lineages (**Figure S1H**), and made much lower contributions to hematopoietic cells at all stages in BM, spleen and thymus (**Figure S1I**). Together with early HSPC accumulation, these functional defects are most consistent with a FL HSPC differentiation block following Dpy30 loss.

To better study the cell-autonomous effect of Dpy30 loss, we established a mixed FL-BM chimeras assay using the *Mx1-cre* mouse model (Kuhn et al., 1995), and induced *Dpy30* excision by injection of Polyinosinic-polycytidylic acid (pIpC) into recipients after stable engraftment of the donor FLs (**Figure 1D**). At two weeks after pIpC injection, *Dpy30* loss had mild or no effects on donor contribution to early HSPCs, but significantly reduced donor contribution to oligopotent HPCs, developing T cells in thymus and B cells in spleen, and mature blood cells in PB (**Figure 1E**), consistent with a multi-lineage differentiation defect. At twelve weeks after pIpC injection, we detected a dramatic reduction in the contribution of the KO donor cells to all cell populations including the HSCs (**Figure 1E**). Taken together,

these results demonstrated an essential role of Dpy30 for FL HSC differentiation and long-term maintenance, similar to its role in adult hematopoiesis (Yang et al., 2016).

Differential and common regulation of gene expression in fetal liver and adult bone marrow HSCs upon *Dpy30* ablation

The largely similar phenotypes of the *Dpy30* KO FL and BM HSCs suggest that Dpy30 and certain Dpy30 targets are fundamentally important in regulating HSCs regardless of the developmental stages. However, we found that Dpy30 loss in FLs did not reduce the expression of some key regulatory genes for adult HSC differentiation and maintenance (Yang et al., 2016), including *Dnmt3a*, *Dnmt3b*, *Etv6*, *Lmo2*, *Sbno2*, *Scl*, and *c-Myc* (**Figure S2A**). To elucidate mechanisms underlying hematopoietic defect in the *Dpy30* KO FLs, we performed RNA-seq on immunophenotypically isolated FL LT-HSCs at E14.5 (**Table S2**). Genes downregulated upon Dpy30 loss in FLs were enriched in a variety of functions, and those upregulated were enriched in membrane proteins and immune functions (**Figure S2B**). In the 275 and 577 genes that were downregulated over two fold upon Dpy30 loss in FL and BM HSCs, respectively, only 21 genes were shared (**Figure S2C**). The number of shared genes increased to 95 when we used 1.5-fold cutoff for downregulation in both types of HSCs (**Figure S2E**). Meanwhile, in the 340 and 669 genes that were upregulated over two fold upon Dpy30 loss in FL and BM HSCs, respectively, 41 genes were shared (**Figure S2D**). The number of shared genes increased to 138 when we used 1.5-fold cutoff for upregulation in both types of HSCs (**Figure S2F**). While no pathways were found to be significantly enriched in the 21 genes commonly downregulated over 2 fold, possibly due to the low number of genes (**Figure S2C**), nucleotide excision repair genes and mitochondrial genes were among those significantly enriched in the 95 genes commonly downregulated over 1.5 fold (**Figure S2E**). On the other hand, inflammation-related genes stood out among the most significantly enriched in the genes commonly upregulated by Dpy30 deficiency either over 1.5 fold or 2 fold in both FL and BM HSCs (**Figures S2D and S2F**).

We next sought to identify Dpy30 targets fundamentally important for HSC regulation by focusing on these commonly up- or down-regulated genes or pathways in both HSCs. In the 21 commonly downregulated genes, 6 (*Acsl6*, *Dnah1*, *Igdcc4*, *Ntpcr*, *Pkn3*, and *Zcchc3*) are relatively highly expressed in HSPCs (**Figure S3A**). We thus sought to study the effects of their depletion in HSPCs by shRNAs on HSPC clonogenicity. We failed to achieve efficient depletion of *Dnah1*, and efficient knockdown of *Zcchc3* or *Pkn3* did not affect formation of any type of colonies (data not shown). Consistent with the specific expression of *Acsl6* in erythrocyte progenitors (**Figure S3A**), *Acsl6* knockdown (**Figure S3B**) specifically impaired formation of BFU-E colonies from FL cells but not other types of colonies (**Figures S3C and**

S3D), suggesting Acsl6 might play a role in red blood cell development rather than in earlier HSC activity. Efficient depletion of *Igdcc4* (sh-1) and *Ntpcr* (sh-1) (**Figure S3B**) significantly impaired the ability of FL cells to form different types of colonies, while inefficient depletion (by the other shRNA) of these genes did not affect colony formation or affected less (**Figures S3C and S3D**). We also observed relative smaller colonies upon *Igdcc4* and *Ntpcr* depletion (**Figure S3D**). We thus further depleted these two genes in adult Lin$^-$ BM cells, and found that depletion of *Igdcc4* and *Ntpcr* (**Figure S3E**) in adult BM cells greatly impaired formation of all different types of colonies (**Figures S3F and S3G**). Taken together, these results demonstrate that Igdcc4 and Ntpcr may play a functional role in early HSPC activity in both fetal and adult hematopoietic systems.

To further identify pathways mediating the regulation of HSCs by Dpy30, we then focused on the commonly upregulated genes. The significant enrichment of inflammatory response suggests cellular stresses upon loss of Dpy30 in both FL and BM HSCs. This is also suggested by the specific and dramatic upregulation of *Cdkn1a* (*p21*) in both types of HSCs as well as BM myeloid progenitors (**Figures 1F, 1G and S2G**), a gene well-known to be induced by a wide spectrum of stress stimuli including genotoxic, metabolic, and oxidative insult (Gorospe et al., 1999). Indeed, several genes involved in redox homeostasis, such as *Alox5*, *Cybb* (*Nox2*), and *Xdh*, were commonly upregulated in both types of HSCs upon Dpy30 loss (**Table S2**). Together with the enrichment of DNA repair and mitochondrial genes being commonly downregulated upon Dpy30 loss, these results prompted us to further study the effect of Dpy30 loss on the metabolic state and DNA integrity of HSCs.

Dpy30 is important for glucose metabolism in HSPCs through direct regulation of key glycolytic genes

Consistent with metabolic stress, both immunoblotting and flow cytometry analyses showed a strong increase in phosphorylation of AMPK at Thr172, a well-established sensor and responder of low nutrient or energy(Lin and Hardie, 2018), in essentially all different cell populations of the hematopoietic system following Dpy30 loss (**Figures 2A and 2B**). Moreover, phosphorylation of Acetyl-CoA carboxylase (Acc) at Ser79, one of AMPK's substrates upon AMPK phosphorylation and activation, was also found to be increased in Dpy30-deficient BM (**Figure 2A**). These results suggest an activation of the cellular sensor of low nutrient or energy in response to Dpy30 deficiency.

We then examined the impact of deficiency of Dpy30 and H3K4 methylation on glucose metabolism, a major constituent of cellular energy pathway. We found that Dpy30 loss in BM HSCs resulted in downregulation of several genes that encode key enzymes in the glycolytic pathway, including a number

of rate-limiting ones, such as hexokinase (Hk1 and Hk2), phosphofructokinase muscle (Pfkm), and pyruvate kinase liver and RBC (Pklr) (**Figure 2C**). Some of these results were confirmed in BM LSK cells and FL HSCs (**Figure S4**). Our chromatin immunoprecipitation assays showed that Dpy30 bound to the transcription start sites of these genes in the Lin$^-$ BM cells in the control mice, but the binding was significantly reduced in the KO littermates (**Figure 2D**). Moreover, H3K4me3 was enriched at the transcription start sites of these genes in the control mice, and such enrichment was dramatically reduced in the KO littermates (**Figure 2E**). These results indicate that Dpy30, through its biochemical activity in facilitating H3K4 methylation, directly regulates the expression of these key glycolytic genes.

Hexokinase phosphorylates glucose to form glucose 6-phosphate. This reaction is important in promoting continuous uptake of glucose into the cell, because it keeps the glucose concentration low and also prevents glucose from diffusing out of the cell due to the added charge of the reaction product. We thus predicted that downregulation of *Hk1* and *Hk2* would impair glucose uptake. Indeed, as measured by glucose analog (2-NBDG) uptake by sorted LSK cells, we found that glucose uptake was consistently impaired in HSPCs by Dpy30 deficiency (**Figure 2F**). This impairment is probably not a result of reduced glucose transporter expression, as our gene expression profiling (**Table S2**) did not show any significant downregulation of known glucose transporter genes.

Transient and modest rescue of hematopoiesis by restoring *Pklr* expression in *Dpy30* KO mice

As one of the rate-limiting enzymes in glycolysis, PKLR catalyzes the transphosphorylation of phosphoenolpyruvate into ATP and pyruvate, a key intermediate in multiple metabolic pathways. Genetic alterations of PKLR are the common cause of chronic hereditary nonspherocytic hemolytic anemia (Zanella et al., 2005). We thus hypothesized that the profound loss of H3K4me3 and expression of *Pklr* in the *Dpy30* KO HSCs was one of the key mechanisms underlying the defective hematopoiesis. To test this hypothesis, we transduced the *Mx1-Cre*; *Dpy30*$^{F/-}$ BM cells with a viral construct expressing *Pklr* and transplanted these cells into recipient mice, which were injected with pIpC to induce *Dpy30* deletion (**Figure 2G**). We found that *Pklr* expression (more than 40 fold over the endogenous level, **Figure S5A**) did not affect the donor contribution to any hematopoietic cell populations before *Dpy30* was deleted, but significantly (but partially) rescued the contribution of the *Dpy30*-deleted donors to early HSPCs (BM LSK) and B cells in the peripheral blood 2 weeks after *Dpy30* deletion (**Figures 2H and S5B**). However, at 3 months after *Dpy30* deletion, we failed to observe any rescue for any cell populations (**Figure S5B**). The transient and partial rescue of hematopoiesis suggests that regulation of *Pklr* expression by Dpy30 functionally contributes to, but is far from the entirety of, the hematopoietic control by Dpy30.

Dpy30 regulates oxidative energy metabolism of the stem cells

Considering the dysregulation of genes involved in redox homeostasis, we next examined the impact of Dpy30 deficiency on oxidative energy metabolism. Real-time measurement of oxygen consumption showed that Dpy30 deficiency significantly reduced both the basal and the total oxidative capacity of Lin^- progenitors (**Figure 3A**). Meanwhile, extracellular acidification rate was also significantly reduced (**Figure 3B**). These results indicate a reduction in oxidative phosphorylation in Dpy30-deficient HPCs. We also found that Dpy30 deficiency in early HSPCs, including LT-HSCs, ST-HSCs, and RLPs, led to substantial reduction in mitochondrial membrane potential, while having little or only modest effects on the mitochondrial mass or DNA level (**Figures 3C-3F and S6A-6C**). Interestingly, Dpy30 loss in the lineage-committed BM cells led to marked increase in mitochondrial membrane potential as well as mass (**Figures S6A and S6B**). Consistent with these results, the level of reactive oxygen species (ROS) was significantly reduced upon Dpy30 loss in early HSPCs including HSCs, but increased in more downstream cells (**Figures 3F and S6C**). Partially consistent with BM cells, FL cells showed significant reduction in ROS levels upon Dpy30 loss in all different hematopoietic cell populations including early HSPCs and Lin^+ cells (**Figure S6D**), while primary mouse embryonic fibroblasts (MEFs) showed minimal alteration in ROS level upon Dpy30 loss (**Figure S6E**). All these results indicate that Dpy30 plays an important role in maintaining the activity of mitochondria and the oxidative energy metabolism. We found that the cellular ATP level was not significantly affected by Dpy30 deficiency (**Figure 3G**). While NADP/NADPH ratio was unaffected, NAD^+/NADH ratio was modestly but significantly increased (**Figure 3H**), suggesting a dysregulated redox homeostasis in Dpy30-deficient HSPCs.

Dpy30 regulates the quiescent state of the stem cells

Considering the intimate connection of HSC energy state and its cell cycle regulation, we further studied how Dpy30 deficiency might affect the HSC cell cycle. We previously showed that Dpy30 deficiency did not significantly affect the proliferative capacity of HSCs or LSK cells as measured by short-time incorporation of nucleotide analog BrdU (Yang et al., 2016). Here we analyzed the proliferative state of the HSCs by staining of Ki-67, a nuclear protein not only strictly associated with cell proliferation (Scholzen and Gerdes, 2000) but also functionally crucial for successful cell division via supporting the structural integrity of mitotic chromosomes (Cuylen et al., 2016). Dpy30 deficiency resulted in significant reduction in the percentage of HSCs in G_0 stage of the cell cycle, as indicated by the lack of Ki-67 expression (**Figures 3I and 3J**). Percentage of HSCs in the S/G2/M phase was not significantly affected (**Figure 3J**). These results suggest that Dpy30-deficient HSCs were in an aberrant and more deeply quiescent state of cell cycle compared to the control HSCs.

Dpy30 and H3K4 methylation are important for genome integrity of cells

We then turned our attention to genotoxic stress upon Dpy30 loss. We found a significant increase in the γ-H2AX level in the FL and Lin$^-$ BM cells upon Dpy30 loss (**Figure 4A**), suggesting breach of genome integrity and increase in DDR. We also directly demonstrated a dramatic and significant increase in DNA breaks following Dpy30 loss in early HSPCs in the BM by using the comet assay (**Figures 4B and 4C**).

Since the major source of DNA damage, ROS, was not increased in *Dpy30* KO HSCs (**Figure 3F**), we sought to determine if the increase in DNA damage could be a result of poor resolution of damage in the absence of Dpy30. To avoid the complication by non-cell-autonomous and cumulative effects for cells derived from the Dpy30-deficient mice, we sought to study DNA repair in the primary MEFs isolated from *Dpy30*$^{F/F}$ and *CAG-CreER; Dpy30*$^{F/F}$ mice. Treatment of the latter cells with 4-OH tamoxifen induced the nuclear translocation of the Cre recombinase to excise *Dpy30* and led to profound reduction in *Dpy30* mRNA level (**Figure 4D**) and global H3K4 methylation (**Figure 4F** and immunoblotting results shown before (Yang et al., 2018)). As shown by the quantification of nuclear γ-H2AX foci at different times after ionizing radiation (**Figures 4E and 4F**), a high level of DNA damage was observed in all cells at 15 minutes after radiation and then gradually reduced to the background level by 24 hours, reflecting the process of DNA repair after damage. We found that the 4-OH tamoxifen-treated *CAG-CreER; Dpy30*$^{F/F}$ MEFs (Dpy30-depleted) accumulated similar level of DNA damage as the 4-OH tamoxifen-treated *Dpy30*$^{F/F}$ MEFs and the vehicle-treated *CAG-CreER; Dpy30*$^{F/F}$ MEFs (both control) at 15 minutes after radiation, but exhibited significantly higher levels of DNA damage than the other two groups of MEFs at 2 hours and 24 hours after radiation (**Figures 4E and 4F**). These results indicate that, while there is no evidence for increase in the source of DNA damage, the DNA repair capacity is significantly impaired in cells deficient of Dpy30 and H3K4 methylation, thus conceivably leading to sustained DNA damage and DDR.

Inhibition of DDR partially rescues the function of the Dpy30-deficienct HSPCs

To determine if DNA damage or the response to DNA damage plays a role in the stem cell function, we studied the colony formation abilities of Lin$^-$ BM cells isolated from *CAG-CreER; Dpy30*$^{F/F}$ mice. We found that 4-OH tamoxifen treatment of these cells greatly reduced their *Dpy30* expression (**Figure 5A**) and capacity in forming all different types of colonies (**Figures 5B and 5C**). Importantly, while the ATM inhibitor (KU55933) treatment had no effect on the clonogenicity of the vehicle-treated (control) cells, it partially but significantly rescued the ability of the 4-OH tamoxifen-treated (Dpy30-depleted) cells in

forming all different types of colonies (**Figures 5C-5E**). These results suggest that the sustained DDR functionally affects stem cell activities.

We also attempted to rescue the function of the Dpy30-deficient HSC in vivo by suppressing DDR. To this end, we have not been able to rescue the hematopoietic defects of Dpy30-deficienct mice by in vivo administration of ATM inhibitor based on peripheral blood profiling (data not shown). However, the mitochondrial membrane potential, which was reduced by Dpy30 loss, was consistently (though did not reach statistical significance) increased by DDR suppression in the Dpy30-deficient mice, although such increase was mainly mediated by an apparently new population of cells among the phenotypic HSCs in these mice (**Figures 5F-H**). These results suggest a connection of the DDR, energy metabolism, and stem cell function, all under the control of the epigenetic regulator Dpy30.

Induction of p21 is partially responsible for the functional defects of the Dpy30-deficient HSCs

Considering the established role of p21 in regulation of cell cycle and stem cell quiescence in response to metabolic and genotoxic stresses, we next sought to determine if the specific and dramatic elevation of *p21* expression played a role in stem cell inactivation upon Dpy30 loss. We generated *Dpy30*$^{F/F}$*; p21*$^{-/-}$*; Mx1-Cre* mice, which, upon pIpC injection, became *Dpy30* and *p21* double KO in the hematopoietic system. *p21* KO had no effect on the numbers or frequencies of any hematopoietic cell populations when Dpy30 was present. However, upon *Dpy30* deletion, which caused severe accumulation of early HSPCs (**Figures 6A and S7A**), *p21* KO significantly alleviated the aberrant accumulation of phenotypic LSK cells (**Figures 6A and S7A**), although it did not alleviate the defect in mature blood cell populations (data not shown).

To better determine the effect of p21 loss on the function of Dpy30-deficient stem cells, we transplanted donor BM from the *Dpy30*$^{F/F}$*; p21*$^{-/-}$*; Mx1-Cre* and *Dpy30*$^{F/F}$*; p21*$^{+/-}$*; Mx1-Cre* mice in the presence of competitor BM into irradiated recipient mice, and examined the donor contribution to the recipient hematopoiesis at different times following *Dpy30* excision induced by pIpC injection into the recipients (**Figure 6B**). Two weeks after pIpC injection, we found that the recipients transplanted with the *Dpy30*$^{F/F}$*; p21*$^{-/-}$*; Mx1-Cre* BM had noticeably more red blood cells than those with the *Dpy30*$^{F/F}$*; p21*$^{+/-}$*; Mx1-Cre* BM (**Figure 6C, top**). As the hematopoietic system of the irradiated recipient mice was mainly contributed by the donor BM, this result indicates that the hematopoietic functionality damaged by Dpy30 deficiency was partially rescued by the compound deficiency of p21. Consistent with the improved red blood cell generation, the recipients with double KO donor BM had significantly smaller spleen than those with *Dpy30*-KO donor BM (**Figure 6C, middle and bottom**), suggesting that p21 deficiency alleviated

splenomegaly induced by Dpy30 loss. Moreover, at 2 weeks after Dpy30 deletion, the double KO donors contributed significantly more than the *Dpy30* KO donors to a subset of hematopoietic cell populations, including GMP and CLP cells in the BM, B cells in spleen, and B cells and Gr/Mac cells in the periphery blood. At 12 weeks after *Dpy30* deletion, this effect was sustained for the splenic and periphery blood cell populations (**Figures 6D and S7B**). These results support a functional role of p21 in mediating the regulation of HSPCs by Dpy30.

DISCUSSION

Together with our previously published results(Yang et al., 2016), the data in this work support a model for the role of Dpy30 in fetal and adult HSCs through regulation of energy metabolism and genome integrity (**Figure 7**). In normal HSCs, Dpy30, through its biochemical activity in facilitating H3K4 methylation mediated by the associated Set1/Mll complexes, ensures the HSC functionality through multiple pathways. These pathways include expression of key regulatory genes for adult HSC maintenance(Yang et al., 2016) and probably a different set of regulatory genes for fetal HSC maintenance, expression of key metabolic (glycolytic and mitochondrial) genes to maintain robust bioenergetics metabolism and appropriate bioenergetic pathways, and safeguarding genome integrity through promoting efficient DNA repair. In the absence of Dpy30 and efficient H3K4 methylation, expression of genes in many of these pathways is dysregulated, leading to dysregulation of energy metabolism and increase in DNA damage. The impairment in glycolysis may affect HSC maintenance, and the impairment in mitochondrial function may disable HSC activation. These stresses induce responses including p21 and other inflammatory pathways, which will suppress the activity of stem cells and lead to attrition of the stem cell in the long term.

Our analyses began with comparing the phenotypes and gene expression alterations upon Dpy30 loss in FL and BM HSCs. In both developmental stages of hematopoiesis, Dpy30 deficiency results in highly similar cellular phenotypes, including a marked accumulation of early phenotypic HSPCs but depletion of more downstream HPCs and multi-lineage mature cells. In competitive transplant assays, the phenotypic HSPCs are functionally defective in giving rise to downstream cells, and also persist for only short period of time before eventually vanishing. Dpy30 loss also disrupts the normal transition of gene expression program between upstream and downstream hematopoietic cells in BM. All of these phenotypes are most consistent with a differentiation block and a defective long-term maintenance of the Dpy30-deficient early HSPCs. The reduction in proliferation of FL RLP and Lin^+ cells may also contribute to the severe depletion of these cell populations in Dpy30-deficient FLs.

We note that our gene analyses for BM used cells from donor-derived cells in the transplant recipients (Yang et al., 2016), while those for FL here used cells in a homeostatic setting without transplant. As a result, the commonly affected genes by Dpy30-deficiency in both FL and BM HSCs identified in this work are likely underestimated. However, they represent genes that are truly responsive to Dpy30 loss regardless of developmental stage or homeostatic/transplant settings, and are thus particularly valuable for identification of the fundamental pathways mediating HSC regulation by Dpy30. These genes are likely important in mediating the effect of Dpy30, but may alternatively reflect a compensatory effect following Dpy30 loss and alteration of certain important biological pathways. Both scenarios provide information regarding the key changes of the cells.

Among the multiple pathways that Dpy30 critically regulates in HSPCs, energy metabolism and DDR stand out as the major pathways that contribute to the effect of this epigenetic modulator in HSPCs. Dpy30 directly regulates the expression of multiple key glycolytic genes, including *Pklr*, (mostly missense) mutations in which are a major cause of hereditary non-spherocytic haemolytic anaemia(Zanella et al., 2005). Our data indicate that Pklr restoration could partially and transiently alleviate the depletion of early HSPCs (LSK cells) and a subset of mature cells (B cells) caused by Dpy30 deficiency. Although we did not know if its expression was sustained at the later time point in this assay, these results suggest that Pklr is merely one of the multiple factors in the metabolic pathways that would need to be restored for a proper energy metabolism required for the normal HSPC activity.

The common upregulation of a number of enzymes in oxidative metabolism in both FL and BM HSCs following Dpy30 deficiency is likely a compensatory response to the impaired mitochondrial function. The overall level of ATP was not significantly perturbed in Dpy30-deficient HSCs, likely due to compensatory responses from other pathways. As Acc is a negative regulator of fatty acid oxidation (Viollet et al., 2009) and is inhibited by its phosphorylation, the increase in Acc phosphorylation (**Figure 2A**) suggests that fatty acid catabolism was elevated to compensate for the impaired energy production in Dpy30-deficient cells. However, the unaffected ATP level makes it unlikely that the HSC dysfunction is a result of reduced total cellular energy level. Rather, we favor the possibility that the altered usage of bioenergetics pathways affects the HSC functionality. Dpy30 deficiency appears to lead to a deeper quiescence of the HSCs based on the cell cycle entry. As quiescent HSCs are known to rely on glycolysis but increase oxidative phosphorylation and energy production upon activation (Kohli and Passegue, 2014; Yu et al., 2013), our results suggest that Dpy30 plays important role in enabling HSC activation by ensuring metabolic reprogramming at the chromatin level.

A number of mouse models with deleted chromatin modulators (Liu et al., 2009; Santos et al., 2014; Tasdogan et al., 2016) and consequent HSPC defects exhibit increase in DDR and ROS level, and the excessive ROS level was shown to be a major contributor to the altered HSPC activity. Consistent with an increase in ROS upon depletion of DPY30 in human fibroblast cells (Simboeck et al., 2013), our results here demonstrate that the ROS level was increased in differentiated adult cells. However, we found a marked reduction of ROS in early HSPCs in the adult stage and in all hematopoietic cells in the prenatal stage upon depletion of Dpy30 and H3K4 methylation, consistent with the reduced mitochondrial activity. Loss of Setd1a, one of the catalytic subunits of the Set1/Mll complexes responsible for the bulk level of cellular H3K4 methylation, also leads to decrease in ROS in HSCs, although the effect on mitochondrial function was not examined (Arndt et al., 2018). We do not yet know the functional impact of a ROS level lower than the normal range on stem cell activity. It appeared that the Dpy30-deficient HSCs in both FL and BM made an effort to increase ROS level by upregulating expression of ROS-producing enzymes, including Alox5, Cybb, and Xdh, suggesting a need to maintain a certain level of ROS for normal HSC function. This is consistent with previous findings that moderate levels of intracellular ROS are needed to activate DNA repair pathway and maintain genomic stability in stem cells (Li and Marban, 2010), and also to support HSC proliferation, differentiation, and mobilization (Chaudhari et al., 2014).

The important function of Dpy30 and H3K4 methylation in efficient DNA repair is likely mediated through two non-exclusive mechanisms. First, Dpy30 and H3K4 methylation are important for appropriate expression of certain DNA repair genes. This echoes the finding that deficiency in Setd1a also impairs DNA repair capacity and results in increased DNA breaks, probably as a result of downregulation of multiple genes important for DNA repair (Arndt et al., 2018). Second, H3K4 methylation may directly regulate DNA repair through impact on the chromatin setting at the damaged sites. H3K4 methylation plays an important role in efficient DNA repair in yeast (Faucher and Wellinger, 2010) and *C. elegans* (Herbette et al., 2017), but is also thought to predispose chromatin for DNA double stranded breaks in mammalian cells through decondensing local chromatin (Burman et al., 2015). As Dpy30-associated H3K4 methylation is functionally important for chromatin accessibility (Yang et al., 2018), it may thus regulate the efficiency of DNA repair by promoting the accessibility of DNA repair proteins. In addition to facilitating DNA repair, H3K4 methylation mediated by Setd1a (and Dpy30) may also protect nascent DNA from degradation in replication stress (Higgs et al., 2018), thereby contributing to the maintenance of genome stability. Our results also suggest that it is the response to DNA damage, rather than the damage itself, that results in the inactivity of HSPCs. While suppression of DDR can temporarily rescue

the function of stem cells, we speculate that it would have a long-term consequence on the system with uncleansed stem and progenitor cells containing damaged genetic information.

In line with p21 being important in maintaining HSC quiescence (Cheng et al., 2000), its level is uniquely (among all CKD inhibitors) and greatly elevated in the Dpy30-deficient HSCs in both FL and BM, keeping the cells in aberrantly deep quiescence regarding the cell cycle entry. Removing this quiescence maintenance factor helps release the Dpy30-deficient HSCs from the deep quiescence and partially enables them to be activated and contribute to the hematopoietic reconstitution after transplant. Similar to the DDR inhibition, we speculate that such release would be mutagenic in the long term of the animals' life span. The incomplete rescue of Dpy30-deficient donor contribution to hematopoietic reconstitution by *p21* KO suggests that, although p21 is an established effector of metabolic and genotoxic stresses, these stresses upon Dpy30 loss may lead to stem cell dysfunction through other effectors. For example, mitochondrial inactivation can lead to HSC defects through metabolite imbalances and epigenetic dysregulation (Anso et al., 2017). Our data also suggest that certain targets of Dpy30, including Igdcc4 and Ntpcr, are important for clonogenicity of both fetal and adult HSCs. Thus, the marked downregulation of these two genes, among other genes, is conceivably a contributor to the reduced stem cell activity in fetal and adult hematopoiesis.

Taken together, our results demonstrate a profound control of stem cell fate determination by a key chromatin modulator via regulating energy metabolism and genome integrity. We still do not clearly know the functional interplay among the metabolic regulation, ROS level, DDR, and the stem cell activities, which warrants further studies. As we previously showed a critical role of Dpy30 in *MLL*-rearranged leukemogenesis (Yang et al., 2014) and Myc-driven lymphomagenesis (Yang et al., 2018), it will be of great interest to investigate whether and how loss or inhibition of this key epigenetic modulator affects cellular metabolism and genome integrity as part of mechanisms underlying cancer inhibition.

MATERIALS AND METHODS

Animals and cells

All animal procedures were approved by the Institutional Animal Care and Use Committee at the University of Alabama at Birmingham. All mice were maintained under specific pathogen free conditions and housed in individually ventilated cages. *Dpy30*$^{+/-}$ mice were generated in our laboratory as previously reported (Yang et al., 2016) and were crossed to *Mx1-Cre* (The Jackson Laboratory, JAX 003556), and *Vav-Cre* (The Jackson Laboratory, JAX 008610) mice to produce *Cre; Dpy30*$^{+/-}$ Mice. These mice were

further crossed with *Dpy30*$^{F/F}$ mice to produce *Cre; Dpy30*$^{F/+}$ and *Cre; Dpy30*$^{F/-}$ littermates for experimental use. All transplant recipient mice were C57Bl/6J and CD45.1^{+}, and purchased from Charles River Laboratories. *P21*$^{-/-}$ (*129S2-Cdkn1atm1Tyj/J*) mice (The Jackson Laboratory, JAX 003263) were further crossed with *Mx1-Cre* and *Dpy30*$^{F/F}$ to generate the littermates of *Dpy30*$^{F/F}$; *P21*$^{+/-}$; *Mx1-Cre* and *Dpy30*$^{F/F}$*; P21*$^{-/-}$ *; Mx1-Cre*.

Primary mouse embryonic fibroblasts (MEFs) were isolated from E13.5 embryos of *Dpy30*$^{F/F}$ or *CAG-CreER; Dpy30*$^{F/F}$ genotype, cultured in MEF culture medium (Dulbecco's Modified Eagle Medium [DMEM] supplemented with L-glutamine, 10% FBS, 0.1 mM non-essential amino acids, and 55μM β-mercaptoethanol, all from Invitrogen), and passage was kept at minimum. MEFs were treated with vehicle (ethanol) as control or 0.5 μM of 4-OH tamoxifen for 4 days to induce *Dpy30* deletion. To induce DNA damage, MEFs were irradiated with 3.2 Gy (X-RAD 320 irradiator; dose rate, 0.8 Gy/min). Post-irradiation incubation time varied from 0 to 24 hours. Immunostaining was performed using primary antibody for H3K4me3 described before(Jiang et al., 2011; Yang et al., 2015) followed by Alexa Fluor 555 Goat anti-Rabbit IgG (H+L) Cross-Adsorbed secondary antibody (ThermoFisher Scientific, # A-21428), and primary antibody for phosphor-H2AX (Ser139) (Millipore, #05-636), followed by Alexa Fluor 488 Goat anti-Mouse IgG (H+L) Cross-Adsorbed secondary antibody (ThermoFisher Scientific, # A-11001).

Retroviral bone marrow transduction and transplantation assays

For competitive transplantation assays, the donor FLs were separated from E14.5 embryos (CD45.2+, *Vav-Cre; Dpy30*$^{F/+}$ and *Vav-Cre; Dpy30*$^{F/-}$) and suspended in phosphate-buffered saline (PBS) supplemented with 3% heat-inactivated fetal bovine serum (FBS), followed by removal of red blood cells. 1×10^6 donor FLs (CD45.2^{+}) and 2×10^5 whole BM cells (C57Bl/6J, CD45.1^{+}) at a ratio of 5:1 were transplanted via tail vein into lethally irradiated recipient mice (CD45.1^{+}). For mixed chimera assays, 1×10^6 whole FLs as donors prepared from E14.5 embryos (CD45.2+, *Mx1-Cre; Dpy30*$^{F/+}$ and *Mx1-Cre; Dpy30*$^{F/-}$) were mixed with 2×10^5 whole BM cells (C57Bl/6J, CD45.1^{+}) at a ratio of 5:1, and transplanted into recipient mice in the same way as described above. Recipients were then injected with 150μl pIpC (InvivoGen) at 1 mg/ml 4 times over 10 days starting at 5 weeks post transplantation. The first two injections were 2 days apart and last injections were 4 days apart. Reconstitution levels were assessed at different time points after pIpC injection. Prior to transplant, all of the recipient mice were lethally irradiated with a split dose of 1100 Rads with 3 hours apart. Donor contribution was determined by flow cytometry at different time points and calculated by CD45.2^{+}/(CD45.1^{+} + CD45.2^{+}) × 100% within the indicated cell type except for the Pklr rescue assay, where the donor contribution was calculated by GFP^{+}/(GFP^{+} + CD45.1^{+}) × 100%. For the Pklr rescue assay, the mouse *Pklr* cDNA was cloned with N-

terminal FLAG tag into pMSCV-IRES-GFP (Addgene, #20672) between EcoRI and XhoI sites to generate the FLAG-*Pklr*-expressing plasmid. To generate the retroviruses, 293T cells were transiently transfected with either empty pMSCV-IRES-GFP vector or the FLAG-*Pklr*-expressing construct with pCL-Eco plasmid using Lipofectamine 2000 (Invitrogen), and viruses in the supernatants were harvested two days after transfection. Four days after injecting both *Dpy30*$^{F/+}$*; Mx1-Cre* and *Dpy30*$^{F/-}$; *Mx1-Cre* mice (6-8-week old) with 150 mg/kg 5-fluorouracil (5-FU, Sigma-Aldrich), BM cells were flushed from these mice and were incubated overnight in RPMI 1640 with 20% fetal calf serum, 20 ng/ml SCF, 20 ng/ml Flt-3, 10 ng/ml IL-3 and 10 ng/ml IL-6 (all from Peprotech, Rocky Hill, NJ) at 37ºC to promote cell cycle entry. Cells were then spinoculated with retroviral supernatant in the presence of 8 µg/ml polybrene (Clontech, Mountain View, CA) for 90 minutes at 500 x g at 30°C. Immediately after spinoculation, 4×10^5 infected cells (CD45.2$^+$) and 2×10^5 helper BM cells (CD45.1$^+$) for a ratio of 2:1 were transplanted via tail vein into lethally irradiated recipient mice (CD45.1$^+$).

Flow cytometry for analysis and cell isolation

Single cell suspensions were prepared from FL, BM, thymus, spleen, or peripheral blood and stained with antibodies as previously described (Yang et al., 2016). FACS analysis was performed on LSRFortessa (Becton Dickinson), and data were analyzed using FlowJo software (Tree Star) as previously described (Yang et al., 2016). To measure phospho-AMPK Cells were then fixed, permeablized and immunostained with anti-phospho-AMPKα (Thr172) antibody (Cell Signaling Technology, #2535). Mean fluorescence intensity was determined by FACS. To measure mitochondrial membrane potential and mitochondrial mass, the HSC staining was modified to make the channels available for tetramethyl rhodamine methyl ester (TMRM) and Mitotracker Deep Red staining (all from Molecular Probes), respectively. After antibody staining cells were incubated with 25 nM TMRM or 1nM Mitotracker Deep red for 15 min at 37ºC followed by flow-cytometry on LSRFortessa (Becton Dickinson), respectively. To measure cellular ROS levels, cells were incubated with 5 mM 2`-7`-dichlorofluorescein diacetate (DCFDA) at 37ºC for 15 min after being stained with the antibodies as described. ROS levels in the gated populations were quantified using flow cytometry. To measure the glucose uptake, 3×10^4 sorted BM LSK cells were incubated with 100 µM 2-NBDG at 37ºC for 1 hour in RPMI-1640 (Life Technologies, no glucose) containing 10% FBS, 100 ng/mL SCF and 100 ng/mL Flt-3. Cellular glucose uptake levels were quantified using flow cytometry. FACS sorting from BM cells was performed as we previously described (Yang et al., 2016). FACS sorting from FLs was performed on LSRAria II (Becton Dickinson). Briefly, 2-3 embryos were pooled and stained with lineage cocktail containing biotin-conjugated antibodies against CD3e (145-2C11), CD4 (GK1.5), CD5 (53-7.3), CD8 (53-6.7), CD45R (RA3-6B2), Gr1 (RB6-8C5) and Ter119 (TER-119), and the following antibodies to discriminate FL HSC:

Sca1 (D7)-PE-Cy7; CD117 (c-Kit 2B8)-PE; CD48 (HM48.1)-FITC; CD150 (TC15-12F12.2)-Pacific blue. All fluorescence-conjugated antibodies were obtained from Biolegend Inc.

Colony formation assay and comet assay

Lin^- FL cells were enriched by staining with lineage cocktail containing biotin-conjugated antibodies against CD3e (145-2C11), CD4 (GK1.5), CD5 (53-7.3), CD8 (53-6.7), CD45R (RA3-6B2), Gr1 (RB6-8C5) and Ter119 (TER-119), and the following anti-biotin microbeads (Milteni Biotec Inc, Cat#:130-090-485). Lin^- BM cells were enriched by Lineage Cell Depletion Kit (Milteni Biotec Inc, Cat#:130-090-858). pLKO.1-based lentiviral constructs expressing scramble control (Addgene plasmid 1864) or short hairpins (shRNAs) targeting indicated genes were transfected into 293T cells, respectively. Viral particles were produced as we described(Yang et al., 2014). Lin^- BM or Lin^- FL cells were harvested as described above and incubated overnight prior to infecting with unconcentrated viruses in the presence of 4 µg/ml of polybrene (Sigma, Missouri). Two days after infection, puromycin (1 µg/ml) was added, and 2 more days later, cells were used for various assays including RNA isolation and colony formation assay. Indicated numbers of cells were plated in duplicate or triplicate into 1.1ml Mouse Methylcellulose Complete Media (STEMCELL Technologies Inc, M3434). Colonies were scored at 7-10 days after plating. Comet Assay was performed using the OxiSelect Comet Assay Kit according to the manufacturer's instructions (Cell Biolabs). Images were acquired by a Nikon Ti-S microscope using a FITC filter, and the percentage of tail DNA of individual cells was determined by the OpenComet (Gyori et al., 2014) plugin of ImageJ. The graph and two-tailed Student's *t*-test were performed using the GraphPad Prism software.

Measurement of oxygen consumption, NAD^+/NADH, $NADP^+$/NADPH, and total ATP level

Measurement of intact cellular respiration was performed using the Seahorse XF24 analyzers. Briefly, the respiration of BM Lin^- cells was measured under basal conditions, in the presence of mitochondrial inhibitor oligomycin (500 nM), mitochondrial uncoupling compound carbonylcyanide - 4-trifluorometh-oxyphenylhydrazone (FCCP) (4 µM), and respiratory chain inhibitor rotenone (1 µM). Sorted BM Lin^- $Sca1^+cKit^+$ (LSK) cells were suspended in PBS and 10,000 cells were added to each well. The ratios of NAD^+/NADH**,** NADP/NADPH and GSH/GSSG were measured with NAD^+/NADH-Glo Assay, NADP/NADPH-Glo Assay and GSH/GSSG-Glo Assay Luminescent Cell Viability Assay kits (all from Promega, Madison, WI), respectively, according to manufacturer's instructions. To determine total cellular ATP levels, BM LSK cells were sorted and assessed using a CellTiter-Glo Luminescent Cell Viability Assay kit (Promega Corporation, Madison, WI).

Proliferation and apoptosis

HSPC proliferation and apoptosis were determined as previously described (Yang et al., 2014; Yang et al., 2016) with modifications. Briefly, to analyze the cell cycle status of FLs, 1.5 mg Brdu was intraperitoneally injected into E14.5 pregnant mice 1 hour prior to sacrifice. Cells were stained with cell surface antibodies as described above and then processed with BrdU staining using the FITC-BrdU Flow kit (BD Pharmingen) following the manufacturer's instructions. The cells were washed by PBS and then stained with antibodies labeled with various fluorochromes as described. For HSC cycle analysis, fresh BM cells were stained with SLAM cell surface markers as described. Cells were then fixed and permeabilized by the buffers from FITC-BrdU Flow kit (BD Pharmingen) and then stained with FITC-labeled anti-Ki67 antibody (BD Biosciences) followed by 7-AAD. Percentages of the cells at G0, G1, and S/G2/M phases were quantified by flow cytometry. For apoptosis assay, cells were harvested and stained with antibodies as described. After washing twice with cold PBS containing 3% heat-inactivated FBS, the cells were then incubated with FITC-Annexin V (BD Pharmingen) and 7-amino-actinomycin D (7-AAD) for 15 minutes in binding buffer (10mM HEPES, 140 mM NaCl and 2.5mM $CaCl_2$) at room temperature in dark. The stained cells were analyzed immediately by flow cytometry.

RNA extraction, chromatin immunoprecipitation (ChIP) and quantitative PCR (qPCR)

Total RNAs were isolated using RNeasy Plus Mini (for non-HSCs) or Micro (for HSCs) Kit (Qiagen) as described (Yang et al., 2016). ChIP assays and qPCR were performed as described(Yang et al., 2016). Primers used are listed in **Table S3**. Relative expression levels were normalized to *Actb*. For ChIP results, percent input was first calculated from ChIP qPCR results as described(Jiang et al., 2011), and ChIP enrichment fold was calculated as the ratio of the percent input value for each locus over that for the negative control site in the control cells (*Mx1-Cre*; *Dpy30*$^{F/+}$). RNAs were reverse transcribed with SuperScript III (Invitrogen). qPCR was performed with SYBR Advantage qPCR Premix (Clontech) on a ViiA7 Real-Time PCR System (Applied Biosystems). Primers used are listed in **Table S3**. Relative expression levels were normalized to *Actb*. RNA-sequencing and analyses were performed as described before(Yang et al., 2016).

Immunoblotting

Whole fetal liver cells and bone marrow cells were isolated after removing red blood cells by ACK lysis buffer. The cells were then lysed by lysis buffer (1% SDS, 10mM EDTA and 50mM Tris-Cl pH 7.5) with fresh added Protease Inhibitor Cocktail (Roche) and boiled for 10 min. Proteins were resolved on SDS-PAGE followed by immunoblotting for Dpy30, H3, H3K4me1, H3K4me2, and H3K4me3, all using antibodies described before (Jiang et al., 2011; Yang et al., 2015), and for β-Actin (Santa Cruz Biotechnology, sc-47778), FLAG (Sigma-Aldrich, F3165), phospho-AMPKα (Thr172) (Cell Signaling

Technology, #2535), phospho-Acc (Ser79) (Cell Signaling Technology, #3661), and phosphor-H2AX (Ser139) (Millipore, #05-636).

Statistics

Unless indicated in the figure legends, the unpaired 2-tailed Student's t-test was used to calculate P values and evaluate the statistical significance of the difference between indicated samples. A P value less than 0.05 was considered significant. Four groups comparison was analyzed by one-factor ANOVA as indicated in figure legends. If ANOVA was overall significant, post hoc *t* test was used for pairwise comparisons of interest.

Data availability

The RNA-seq data have been deposited in Gene Expression Omnibus database with the accession number GSE101856.

ACKNOWLEDGEMENTS

We thank the Comprehensive Flow Cytometry Core (CFCC) at UAB, which are supported by NIH core grants P30 AR048311 and P30 AI027767. The X-RAD 320 irradiator was purchased by the UAB animal facility using NIH Grant G20RR022807. We thank Ying Gai Tusing and Yanfang Zhao for technical assistance with mice work. This work was supported by NIH grant R01DK105531, Start-up funds from the State of Alabama and University of Virginia. HJ is a recipient of the American Society of Hematology Scholar Award, the American Cancer Society Research Scholar Award, and the Leukemia and Lymphoma Society Scholar Award.

AUTHOR CONTRIBUTIONS

Z.Y. and H.J. conceived the project and designed the experiments. Z.Y. conducted most of the experiments and analyzed the results, K.S. conducted some of the experiments and analyzed the results, A.K. conducted bioinformatic analyses. Z.Y. and H.J. wrote the paper.

FIGURE LEGENDS

Figure 1. Dpy30 deficiency in the fetal hematopoietic system results in anemia and defective HSC function.

Vav-Cre; Dpy30$^{F/+}$ (*F*/+) and *Vav-Cre; Dpy30*$^{F/-}$ (*F*/-) littermate fetuses were used in panels (A-C) and (G).

(A) Gross appearance of littermate fetuses at E14.5 and E15.5.

(B) Immunoblotting for different levels of H3K4 methylation and other indicated proteins in fetal liver cells.

(C) Absolute numbers of fetal liver cell populations. n=5 each.

(D) Scheme for the mixed chimera transplantation system using whole fetal liver cells from *Mx1-Cre; Dpy30*$^{F/+}$ or *Mx1-Cre; Dpy30*$^{F/-}$ fetuses as donors and whole BM cells from wild type mice as competitors.

(E) Donor contribution to different cell populations in chimeras at indicated times after pIpC injections as shown in (D). n=4-6 each.

(F and G) Relative expression of key CDK inhibitor genes in the control (*F/*+) versus Dpy30 KO (*F/*–) HSCs in two independent BM chimeras (F) and three fetal livers at E14.5 (G), as analyzed by RNA-seq. The expression levels in *F/*+ cells were set as 1. The BM HSC data are based on RNA-seq results in donor (*Mx1-Cre; Dpy30*$^{F/+}$ or *Mx1-Cre; Dpy30*$^{F/-}$) -derived HSCs in the BM chimera recipients in two independent BM transplantations (TP1 and TP2) from our previous work (Yang et al., 2016).

Data are shown as mean ±SD for (C) and (E). *P<0.05, **P<0.01, ***P<0.001, ****P<0.0001, by 2-tailed Student's *t*-test.

See also Figures S1-S3.

Figure 2. Dpy30 deficiency impairs glucose metabolism in BM HSCs.

(A) Immunoblotting for indicated proteins in whole or Lin$^-$ BMs from pIpC-injected *Mx1-Cre; Dpy30*$^{F/+}$ and *Mx1-Cre; Dpy30*$^{F/-}$ mice. Each lane represents an individual pool of cells.

(B) Representative FACS analyses for phospho-AMPK (Thr172) in different cell populations in BMs from pIpC-injected *Mx1-Cre; Dpy30*$^{F/+}$ and *Mx1-Cre; Dpy30*$^{F/-}$ mice.

(C) Relative expression of glycolytic genes, as analyzed by RNA-seq in two independent BM transplantations from previous work (Yang et al., 2016). Underlined genes are rate-limiting for glycolysis. The expression levels in *F/*+ cells were set as 1.

(D and E) ChIP for Dpy30 (D) and H3K4me3 (E) using Lin$^-$ BM cells from pIpC-injected *Mx1-Cre; Dpy30*$^{F/+}$ and *Mx1-Cre; Dpy30*$^{F/-}$ mice, and shown as mean ± SD. n=3 mice each. *P<0.05, **P<0.01, ***P<0.001, by 2-tailed Student's *t*-test.

(F) Representative histogram showing reduced 2-NBDG uptake in vitro by sorted LSK cells from pIpC-injected *Mx1-Cre; Dpy30*$^{F/+}$ and *Mx1-Cre; Dpy30*$^{F/-}$ mice. The gray line indicates isotype control. Each colored line represents an individual mouse out of a total of 3 mice each.

(G) Scheme for the rescue assay using BMs from *Mx1-Cre; Dpy30*$^{F/+}$ (*F/+*) and *Mx1-Cre; Dpy30*$^{F/-}$ (*F/-*) mice. Both the control and Pklr viral constructs expressed GFP.

(H) Donor contribution to indicated cell populations in the transplant recipients 2 weeks after pIpC-injections. n=4 mice each. Data are shown as mean ±SD. *P<0.05, by 1-factor ANOVA with post hoc *t* test.

See also Figures S4 and S5.

Figure 3. Dpy30 deficiency impairs mitochondrial function and alters quiescence state of the BM HSCs.

BMs from pIpC-injected *Mx1-Cre; Dpy30*$^{F/+}$ (*F/+*) and *Mx1-Cre; Dpy30*$^{F/-}$ (*F/-*) mice were used in this figure.

(A and B) Oxygen consumption rate (OCR) (A) and basal extracellular acidification rates (B) of live Lin$^-$ BM cells were measured. n=3 mice each.

(C, E, and F) Analyses (left) and representative histograms (right) for mitochondrial membrane potential (C), mitochondrial mass (E) and ROS level (F) of indicated BM cell populations. n=3 mice each.

(D) Mitochondrial DNA levels from BM LSK cells were determined by qPCR on *mt-Co2* and normalized to *Hbb* for genomic DNA levels. n=3 mice each.

(G and H) Total cellular ATP levels (G), and NAD$^+$/NADH and NADP$^+$/NADPH ratios (H) in BM LSK cells were determined. n=3 mice each.

(I) Representative FACS plots of Ki67 staining.

(J) G0, G1, and S/G2/M phases of HSCs were quantified. n = 5 mice each.

Data are shown as mean ±SD for all panels. n.s. not significant, *P<0.05, **P<0.01, ***P<0.001, by 2-tailed Student's *t*-test.

See also Figure S6.

Figure 4. Dpy30 deficiency results in increase in DNA damage and impairs DNA repair.

(A) Immunoblotting of γ-H2AX and H3 in *Vav-Cre; Dpy30*$^{F/+}$ and *Vav-Cre; Dpy30*$^{F/-}$ fetal liver cells and Lin^{-} BM cells from pIpC-injected *Mx1-Cre; Dpy30*$^{F/+}$ and *Mx1-Cre; Dpy30*$^{F/-}$ mice.

(B and C) Comet assay using BM LSK cells pooled from 3 mice each, with representative images in (B) and quantification of the relative tailing level of cells in (C). Red arrows point to comet-shaped cells with significant DNA damage. The representative zoom-in images of an undamaged (blue box) and damaged (red box) cells are shown in the insets. In (C), each dot represents a cell analyzed by the OpenComet software, and 100% means maximum tail DNA (most damage) and 0% means tail DNA (no damage). **P<0.01, by 2-tailed Student's *t*-test.

(D-F) Primary MEFs of indicated genotypes were treated with vehicle (ethanol) or 4-OH tamoxifen. Relative *Dpy30* mRNA levels were determined by RT-qPCR and normalized to *Actb*, n=2 for each of the left two bars and n=4 for each of the right two bars (D). MEFs were subjected to ionizing radiation at 0 min, followed by γ-H2AX staining at indicated times after radiation. The γ-H2AX foci numbers per cell from 20-60 cells in each repeat of 3 biological repeats are plotted (E). Representative images of indicated cells at 2hrs post irradiation are shown (F). *P<0.05, ***P<0.001, by 1-factor ANOVA with post hoc *t* test.

Figure 5. Inhibition of DDR partially rescues the function of the Dpy30-deficient hematopoietic cells.

(A-E) Lin^{-} BM cells from *CAG-CreER; Dpy30*$^{F/F}$ mice were treated with indicated agents in liquid culture for two days and subjected to colony formation assays.

(A) Relative *Dpy30* mRNA levels were determined by RT-qPCR and normalized to *Actb.* n=3 each.

(B and C) All colonies (B) (3 independent biological repeats) and different types of colonies (C) (2 independent biological repeats) were quantified.

(D and E) Representative image of the plates (D) and colonies (E) are shown.

(F-H) *Mx1-Cre; Dpy30*$^{F/+}$ *or Mx1-Cre; Dpy30*$^{F/-}$ mice were injected with pIpC and either vehicle (DMSO) or ATM inhibitor KU55933 (F), followed by determination of mitochondrial membrane potential of HSCs by FACS. The FACS plots with the gating for the effect of KU55933 in the KO mice are shown in (G) where individual mouse is represented by the individual line, and the results are quantified in (H), n=3 for each.

Data are shown as mean ±SD for all bar graphs. *P<0.05, **P<0.01, ***P<0.001, by 1-factor ANOVA with post hoc *t* test.

Figure 6. *P21* deletion partially rescues the function of the *Dpy30* KO hematopoietic cells.

(A) Absolute numbers of BM cell populations in pIpC-injected mice of indicated genotypes. n=3 each.

(B) Scheme for the mixed chimera transplantation system using whole BM cells from *Dpy30*$^{F/F}$*; p21*$^{+/-}$*; Mx1-Cre* or *Dpy30*$^{F/F}$*; p21*$^{-/-}$*; Mx1-Cre* mice as donors and whole BM cells from wild type mice as competitors.

(C) Representative whole BMs flushed from long bones (top) and spleens (middle) in recipient mice that received *Dpy30*$^{F/F}$*; p21*$^{+/-}$*; Mx1-Cre* or *Dpy30*$^{F/F}$*; p21*$^{-/-}$*; Mx1-Cre* donor cells at two weeks after pIpC injection. Spleen weights are quantified (bottom). n=4 for each.

(D) Contribution of *Dpy30*$^{F/F}$*; p21*$^{+/-}$*; Mx1-Cre* and *Dpy30*$^{F/F}$*; p21*$^{-/-}$*; Mx1-Cre* donors to different cell populations in BM chimeras at two and 12 weeks after pIpC injection. n=4 for each.

Data are shown as mean ±SD for all bar graphs. *P<0.05, **P<0.01, by 1-factor ANOVA with post hoc *t* test (A) and 2-tailed Student's t-test (C) and (D).

See also Figure S7.

Figure 7. A model for the role of Dpy30 in HSC through regulation of energy metabolism and genome integrity.

(A) Dpy30 normally ensures the functionality of HSC through guarding genome integrity and regulating key maintenance genes. It also enables HSC activation by regulating genes in energy metabolism. Note that Dpy30 probably regulates different set of maintenance genes in the fetal and adult HSCs.

(B) Dpy30 loss results in dysregulation of metabolism and key maintenance gene expression, as well as breach of genome integrity. These stresses induce p21 and other responses that lead to stem cell loss and activation defect.

SUPPLEMENTAL TABLES AND FIGURE LEGENDS

Table S1: Cell surface phenotypes used in this work

Cell population	Cell surface phenotype
Lin$^-$ (Fetal liver)	CD3$^-$ CD4$^-$ CD5$^-$ CD8$^-$ B220$^-$ Gr1$^-$ TER119$^-$
Lin$^-$ (Bone marrow)	CD3$^-$ B220$^-$ CD11b Gr1$^-$ TER119$^-$
Lin$^+$	Cells excluding Lin$^-$
LSK	Lin$^-$Sca1$^+$cKit$^+$
LT-HSC	LSK CD48$^-$CD150$^+$
ST-HSC	LSK CD48$^+$CD150$^+$
RLP	LSK CD48$^+$CD150$^-$
MyePro	Lin$^-$Sca1$^-$cKit$^+$ (L$^-$S$^-$K$^+$)
CLP	Lin$^-$Sca1^{low}cKit^{low}IL7R$^+$CD135$^+$
CMP	Lin$^-$Sca1$^-$cKit$^+$CD34$^+$FcRγ$^-$
MEP	Lin$^-$Sca1$^-$cKit$^+$ CD34$^-$FcRγ$^-$
GMP	Lin$^-$Sca1$^-$cKit$^+$ CD34$^+$FcRγ$^+$
B cell	B220$^+$
T cell	CD3ε$^+$
DN	CD4$^-$CD8$^-$
DP	CD4$^+$CD8$^+$
Gr/Mac	Gr1$^+$ or Mac1$^+$

Table S2. Gene expression analyses in fetal liver HSCs in control and *Dpy30* KO background. This Table is separately attached as an Excel file. There are 14 tabs in this file. Fetal liver (FL) HSCs from 3 pairs of *Vav-Cre; Dpy30*$^{F/+}$ (control) and *Vav-Cre; Dpy30*$^{F/-}$ (KO) fetuses, each pair from the same litter, at E14.5 were sorted out for RNA-Seq. Gene expression data for the bone marrow (BM) HSCs are from our previous work (Yang et al., 2016) and are included here for convenience of comparison. The BM data are from two transplant (TP1 and TP2) recipients at two weeks after pIpC induction. These TP recipients received *Mx1-Cre; Dpy30*$^{F/+}$ (control) and *Mx1-Cre; Dpy30*$^{F/-}$ (KO) donor BM cells and were then injected with pIpC. Compared to control, genes up- or down-regulated more than 2 (or 1.5) fold in both BM TPs are shown in tabs "BM up>2 (or 1.5)" and "BM down>2 (or 1.5)". All normalized FL HSC RNA-Seq data with three fetuses of each genotype are listed in tab "All genes in FL HSC". Genes up- or down-regulated in FL HSCs with mean value more than 2 fold and p <0.05 are listed in tabs "FL down >2" and "FL up>2". Genes up- or down-regulated more than 1.5 fold in all three littermate pairs are listed in tabs "FL down >1.5" and "FL up>1.5". Tabs "BM & FL down>2 (or 1.5)" show overlapping genes between tabs "BM down>2 (or 1.5)" and "FL down >2 (1.5)". Tabs "BM & FL up>2 (1.5)" show overlapping genes between tabs "BM up>2" and "FL up>2".

Table S3: Primers and Oligos

App.	Species	gene	Forward primer (5'-3')	Backward primer (5'-3')
expression	mouse	*Actb*	CCTTCAACACCCCAGCCATGTACG	GGCACAGTGTGGGTGACCCCGTC
expression	mouse	*Acsl6*	ATGCAGAGGAACTCAACTACTG	CTTTGTCCTGTCCTCGTCTTT
expression	mouse	*Cdkn1a*	CTGGGAGGGGACAAGAG	GCTTGGAGTGATAGAAATCTG
expression	mouse	*Dnah1*	GCTGGTACAAGAGGTCATTAGG	CTCGAGCTCCAAGGACATTAC
expression	mouse	*Dnmt3a*	AGCGTCACACAGAAGCATATC	GGCGGTAGAACTCAAAGAAGAG
expression	mouse	*Dnmt3b*	TCTGAGATCTCTGCTGACAAAC	GTGGTACATGGCCTTCCTATAA
expression	mouse	*Dpy30*	ACCCTCACTCTGAGTACGGG	GGACTGTAGATCCACCTTCTGT
expression	mouse	*Etv6*	TGCTCTTCTCACCATTCTTCC	GTCCTCTGGACACAGTTATCTTC
expression	mouse	*Hk1*	CTGGAATCTCCCATCGCTTTAG	GGAAACACCACTCCGACTTT
expression	mouse	*Hk2*	CTCGGCCTTGTGAGTAGATAGA	CGCGGGTGAATGAGGTATTT
expression	mouse	*Igdcc4*	CAAAGCCCTGTGTCCTCTAAC	GCATGTTCCTGAGCCATATCT
expression	mouse	*Lmo2*	TGCGGGTGAAAGACAAAGT	GTCGGAGTTGATGAGAAGGTATC
expression	mouse	*Myc*	CCACCAGCAGCGACTCTGA	TGCCTCTTCTCCACAGACACC
expression	mouse	*Ntpcr*	CAGGAAGGGAAGAGGATAGGA	TCGGGCTTTCCAGGTAGA
expression	mouse	*Pfkm*	GCATCCCATTTGTGGTCATTC	GTCACAGGTTGTGCAGATAGT
expression	mouse	*Pgk1*	CACAGAAGGCTGGTGGATTT	CTTTAGCGCCTCCCAAGATAG
expression	mouse	*Pklr*	GAGTCGGAGGTGGAAATTGT	CCTGGGTGATATTGTGGTAGTC
expression	mouse	*Pkn3*	GGACACAGAAGAGGAGGTATTTG	CTTCTGGAGGAGCTTCTGAATG

expression	mouse	*Sbno2*	CTTGGATGTGGAGAAGGACTG	CGAAGGTGTCGGAGAAGTATTG
expression	mouse	*Scl*	CACCCACCAGACAAGAAACTA	CTCCTCCTGGTCATTGAGTAAC
expression	mouse	*Zcchc3*	GAAGACCCTCTTCATCCTCTTC	GAACCTGTCGGTCACTTTCA
expression	mouse	*Hbb*	GAAGCGATTCTAGGGAGCAG	GGAGCAGCGATTCTGAGTAGA
expression	mouse	*mt-Co2*	GCCGACTAAATCAAGCAACA	CAATGGGCATAAAGCTATGG
App.	**Species**	**gene**	**Forward primer (5'-3')**	**Backward primer (5'-3')**
shRNA	mouse	*Scramble*	CCGGCCTAAGGTTAAGTCGCCCTCGCTCGAGCGAGGGCGACTTAACCTTAGGTTTTTG	AATTCAAAAACCTAAGGTTAAGTCGCCCTCGCTCGAGCGAGGGCGACTTAACCTTAGG
shRNA (1#)	mouse	*Acsl6*	CCGGTGCACGGTAATCGTCGATAAACTCGAGTTTATCGACGATTACCGTGCATTTTTG	AATTCAAAAATGCACGGTAATCGTCGATAAACTCGAGTTTATCGACGATTACCGTGCA
shRNA (2#)	mouse	*Acsl6*	CCGGGCAAAGGAGAAGGAGAGATATCTCGAGATATCTCTCCTTCTCCTTTGCTTTTTG	AATTCAAAAAGCAAAGGAGAAGGAGAGATATCTCGAGATATCTCTCCTTCTCCTTTGC
shRNA (1#)	mouse	*Dnah1*	CCGGCGAGCATATCAATCCTGACAACTCGAGTTGTCAGGATTGATATGCTCGTTTTTG	AATTCAAAAACGAGCATATCAATCCTGACAACTCGAGTTGTCAGGATTGATATGCTCG
shRNA (2#)	mouse	*Dnah1*	CCGGCGAGGCGTCATCAGAAATTAACTCGAGTTAATTTCTGATGACGCCTCGTTTTTG	AATTCAAAAACGAGGCGTCATCAGAAATTAACTCGAGTTAATTTCTGATGACGCCTCG
shRNA (1#)	mouse	*Igdcc4*	CCGGGCGAGCAAATCATTGGCTTCTCTCGAGAGAAGCCAATGATTTGCTCGCTTTTTG	AATTCAAAAAGCGAGCAAATCATTGGCTTCTCTCGAGAGAAGCCAATGATTTGCTCGC
shRNA (2#)	mouse	*Igdcc4*	CCGGCCATTTACCAAGTACGAGTTTCTCGAGAAACTCGTACTTGGTAAATGGTTTTTG	AATTCAAAAACCATTTACCAAGTACGAGTTTCTCGAGAAACTCGTACTTGGTAAATGG
shRNA (1#)	mouse	*Ntpcr*	CCGGGCGGTTTGAGTAAATTCTAAACTCGAGTTTAGAATTTACTCAAACCGCTTTTTG	AATTCAAAAAGCGGTTTGAGTAAATTCTAAACTCGAGTTTAGAATTTACTCAAACCGC
shRNA (2#)	mouse	*Ntpcr*	CCGGCCAAACACAGAGTGTGTATCACTCGAGTGATACACACTCTGTGTTTGGTTTTTG	AATTCAAAAACCAAACACAGAGTGTGTATCACTCGAGTGATACACACTCTGTGTTTGG
shRNA (1#)	mouse	*Pkn3*	CCGGCGCTATCAAGGCGTTGAAGAACTCGAGTTCTTCAACGCCTTGATAGCGTTTTTG	AATTCAAAAACGCTATCAAGGCGTTGAAGAACTCGAGTTCTTCAACGCCTTGATAGCG
shRNA (2#)	mouse	*Pkn3*	CCGGGACACAGAAGAGGAGGTATTTCTCGAGAAATACCTCCTCTTCTGTGTCTTTTTG	AATTCAAAAAGACACAGAAGAGGAGGTATTTCTCGAGAAATACCTCCTCTTCTGTGTC
shRNA (1#)	mouse	*Zcchc3*	CCGGGACGACATCTACGCGGTCATTCTCGAGAATGACCGCGTAGATGTCGTCTTTTTG	AATTCAAAAAGACGACATCTACGCGGTCATTCTCGAGAATGACCGCGTAGATGTCGTC
shRNA (2#)	mouse	*Zcchc3*	CCGGGCAGCCCAAGACGTGCTTTAACTCGAGTTAAAGCACGTCTTGGGCTGCTTTTTG	AATTCAAAAAGCAGCCCAAGACGTGCTTTAACTCGAGTTAAAGCACGTCTTGGGCTGC
App.	**Species**	**gene**	**Forward primer (5'-3')**	**Backward primer (5'-3')**
genotyping	mouse	*Dpy30*	TTCAGCACCAGCACTTGGATTTGG (within 5' arm)	CCAACTGACCTTGGGCAAGAACAT (targets "-" allele)
genotyping	mouse	*Dpy30*		GCACAGCAAGTCCCTGTAATA (within exon 4)
genotyping	mouse	*Dpy30*	CCAGGACTAAAGGCGCATAA (targets "FC" allele)	GCCAAGGCTACACAGAGAAA (within 3' arm)
App.	**Species**	**gene**	**Forward primer (5'-3')**	**Backward primer (5'-3')**
Chip	mouse	*Hk1* (TSS-273bp)	TCAGAGGGAAGTGGGATAGAG	CAGCCCACTAGGTTTCATCTT
Chip	mouse	*Pfkm* (TSS+30bp)	CCAAGCTCAAGACAAGAGGAA	GCTCATCGCCTCTTGGTAAT
Chip	mouse	*Pklr* (TSS+29bp)	CAGATAAGACCAGCAGTTAGGG	GTAGCTCGTTCTCTTGGACAG
Chip	mouse	*Punc* (TSS-4260bp) (*Neg)*	AGCCATGCCATCTCTCTGGTTTCT	CACTTGATGTGCCAGCCAGTTGAA

Figure S1. Dpy30 deficiency in fetal liver results in anemia and defective HSC function.

Vav-Cre; Dpy30$^{F/+}$ (*F*/+) and *Vav-Cre; Dpy30*$^{F/-}$ (*F*/-) littermate fetuses were used in all panels.

(A) Genomic PCR to detect *Dpy30* deletion in total fetal liver at E14.5. The calculated sizes of the PCR products (shown on the right) are consistent with the mobility of the bands.

(B) Relative *Dpy30* mRNA levels in whole fetal liver cells determined by RT-qPCR and normalized to *Actb*. n=3-6 each.

(C) Percentage of different cell populations in fetal liver. Data are shown as mean ±SD. n=5 each.

(D) Representative FACS analysis of fetal liver cells at E14.5.

(E) BrdU incorporation (left) and annexin V staining (right) assays for different cell populations in fetal liver at E14.5. Data are shown as mean ±SD. n=4-6.

(F) Colony formation assay using 40,000 fetal liver cells. A presentative image of the plates with formed colonies is shown on left. n=3 each.

(G) Scheme for the competitive transplantation system using whole fetal liver cells from *Vav-Cre*; *Dpy30*$^{F/+}$ and *Vav-Cre*; *Dpy30*$^{F/-}$ as donors and wild type BM as competitors.

(H) Donor contribution to indicated peripheral blood cells was determined by FACS at different times post transplantation following the scheme in (e). n=3-5 mice.

(I) Donor contribution to different cell populations in bone marrow (BM), thymus (Thy) and spleen (Spl) at 4 weeks (top) and 12 weeks (bottom) after transplantation. n=4-6 mice.

Data are shown as mean ± SD for all bar graphs and (F). n.s., not significant, **P<0.01, ***P<0.001, ****P<0.0001, ***** P<0.00001, 2-tailed Student's *t*-test.

Related to Figure 1.

Figure S2. Analysis of genes significantly altered by Dpy30 loss in HSCs.

(A) Relative mRNA levels of indicated genes in the HSCs sorted from fetal livers of *Vav-Cre; Dpy30*$^{F/+}$ and *Vav-Cre; Dpy30*$^{F/-}$ littermate fetuses at E14.5 were determined by RT-qPCR and normalized to *Actb*. Data are shown as mean ± SD. n=3 each. n.s., not significant, **** P<0.0001, by 2-tailed Student's *t*-test.

(B) Gene ontology analysis by DAVID for genes that were downregulated (A) or upregulated (B) over 2 fold in HSCs from 3 pairs of fetal littermates.

(C and D) Venn diagram for genes that were downregulated (C) or upregulated (D) over 2 fold in HSCs from 3 pairs of fetal littermates and 2 pairs of BM HSCs (left). Gene ontology analysis by DAVID of the shared genes are shown (right). In panels (C-G), the BM HSC data are based on RNA-seq results in donor (*Mx1-Cre; Dpy30*$^{F/+}$ or *Mx1-Cre; Dpy30*$^{F/-}$) -derived HSCs in the BM chimera recipients in two independent BM transplantations (TP1 and TP2) from our previous work (Yang et al., 2016).

(E and F) Venn diagram for genes that were downregulated (E) or upregulated (F) over 1.5 fold in HSCs from 3 pairs of fetal littermates and 2 pairs of BM HSCs (left). Gene ontology analysis by DAVID of the shared genes are shown (right).

(G) RNA-seq profiles at *Cdkn1a* (*p21*) from one BM chimera transplant assay.

Related to Figure 1.

Figure S3. Functional roles of a small subset of genes commonly downregulated by Dpy30 loss in both FL and BM HSCs.

(A) Shown as output from Gene Expression Commons (https://gexc.standford.edu by Weissman lab).

(B-G) Lin$^-$ cells enriched from wild type E14.5 fetal livers were used in (B-D). Lin$^-$ cells enriched from wild type BM were used in (E-G).

(B and E) Knockdown efficiencies of indicated genes were determined by RT-qPCR and normalized to *Actb*, and shown as mean ± SD as duplicate measurements.

(C-G) Colony numbers of different types colonies were scored at 7 days (C) or 5 days (F) after plating. Data are shown as mean ± SD. *P<0.05, **P<0.01, ***P<0.001, by 2-tailed Student's *t*-test between the control (Scr) and the gene-specific shRNA for the same type of colonies. Representative colonies are shown in (D) and (G). BFU-E, Burst-forming unit-erythroid; CFU-GM&M, colony forming unit-granulacyte, macrophage; GEMM: colony forming unit-granulocyte, erythroid, macrophage, and megakaryocyte.

Related to Figure 1.

Figure S4. Analysis of key glycolytic genes significantly downregulated by Dpy30 loss.

Relative expression of key glycolytic genes in BM LSK cells (A) and FL HSCs (B), as determined by RT-qPCR and normalized to *Actb.* Data are shown for each measurements.

(A) Relative mRNA levels of indicated genes in the donor (*Mx1-Cre; Dpy30*$^{F/+}$ or *Mx1-Cre; Dpy30*$^{F/-}$) -derived LSK cells in the BM chimera recipients in two independent BM transplantations (TP1 and TP2) from previous work (Yang et al., 2016).

(B) Relative mRNA levels of indicated genes in the HSCs sorted from fetal livers of *Vav-Cre; Dpy30*$^{F/+}$ and *Vav-Cre; Dpy30*$^{F/-}$ littermate fetuses at E14.5.

Data are shown for each measurements. *P<0.05, **P<0.01, ***P<0.001, by 2-tailed Student's *t*-test.

Related to Figure 2.

Figure S5. Restored *Pklr* expression partially rescues the functional defect of Dpy30-deficient hematopoietic cells.

(A) Relative expression of FLAG-tagged *Pklr* from retrovirally-transduced BM cells was determined by RT-qPCR (left) and immunoblotting (right) prior to the transplant. The *Pklr* mRNA levels were normalized to *Actb* and relative to the level in the *Dpy30*$^{F/+}$*; Mx1-Cre* + control, and are shown as mean ±SD of technical duplicate. Anti-FLAG antibody was used to detect FLAG-Pklr, as our anti-Pklr antibody failed to react with mouse Pklr.

(B) Donor contribution to indicated cell populations in bone marrow (BM), thymus (Thy), spleen, and peripheral blood (PB) at before deletion (top), 2 weeks (middle) and 3 months (bottom) in the transplant recipients 2 weeks and 3 months after pIpC-injections as well as before injection following scheme in Figure 2G. n=4 each. Data are shown as mean ±SD. *P<0.05, by 1-factor ANOVA with post hoc *t* test.

Related to Figure 2.

Figure S6. Dpy30 deficiency impairs mitochondrial function in different types of cells.

(A-C) Mitochondrial membrane potentials (A), mitochondrial mass (B) and intracellular ROS levels (C) in different BM cell populations from pIpC-injected *Mx1-Cre; Dpy30*$^{F/+}$ (*F/+*) and *Mx1-Cre; Dpy30*$^{F/-}$ (*F/-*) mice were determined by FACS. Because these values were vastly different for MyePro and Lin^{+} cells (much higher) compared to the cell populations, gating criterion for these values were the same for LT-HSC, ST-HSC, RLP, and LSK cells, but different for MyePro, and that for Lin^{+} cells was also different from all other cells. Data are shown as mean ±SD for all panels. n=4 or 3 mice as indicated. n.s., not significant, *P<0.05, **P<0.01, ***P<0.001, by 2-tailed Student's *t*-test.

(D) Intracellular ROS levels in different cell populations of fetal livers of indicated genotypes at E14.5. n=2 each. Data are shown as mean ±SD. n.s., not significant, *P<0.05, **P<0.01, by 1-factor ANOVA with post hoc *t* test.

(E) Primary MEFs of indicated genotypes were treated with vehicle (ethanol) or 4-OH tamoxifen (Tam), and intracellular ROS levels were determined by FACS.

Related to Figure 3.

Figure S7. *P21* deletion partially rescues the function of the *Dpy30* KO hematopoietic cells.

(A) Representative FACS analysis of BM from pIpC-injected mice of indicated genotypes.

(B) Representative FACS analysis of B cells in spleen and granulocytes & macrophages in peripheral blood from the recipient mice that received donors of indicated genotypes (top) based on the scheme in Figure 9b.

Related to Figure 6.

REFERENCES

Anso, E., Weinberg, S.E., Diebold, L.P., Thompson, B.J., Malinge, S., Schumacker, P.T., Liu, X., Zhang, Y., Shao, Z., Steadman, M.*, et al.* (2017). The mitochondrial respiratory chain is essential for haematopoietic stem cell function. Nature cell biology *19*, 614-625.

Arndt, K., Kranz, A., Fohgrub, J., Jolly, A., Bledau, A.S., Di Virgilio, M., Lesche, M., Dahl, A., Hofer, T., Stewart, A.F.*, et al.* (2018). SETD1A protects HSCs from activation-induced functional decline in vivo. Blood *131*, 1311-1324.

Blanpain, C., Mohrin, M., Sotiropoulou, P.A., and Passegue, E. (2011). DNA-damage response in tissue-specific and cancer stem cells. Cell stem cell *8*, 16-29.

Burman, B., Zhang, Z.Z., Pegoraro, G., Lieb, J.D., and Misteli, T. (2015). Histone modifications predispose genome regions to breakage and translocation. Genes & development *29*, 1393-1402.

Chaudhari, P., Ye, Z., and Jang, Y.Y. (2014). Roles of reactive oxygen species in the fate of stem cells. Antioxidants & redox signaling *20*, 1881-1890.

Cheng, T., Rodrigues, N., Shen, H., Yang, Y., Dombkowski, D., Sykes, M., and Scadden, D.T. (2000). Hematopoietic stem cell quiescence maintained by p21cip1/waf1. Science (New York, N.Y.) *287*, 1804-1808.

Ciccia, A., and Elledge, S.J. (2010). The DNA damage response: making it safe to play with knives. Molecular cell *40*, 179-204.

Cuylen, S., Blaukopf, C., Politi, A.Z., Muller-Reichert, T., Neumann, B., Poser, I., Ellenberg, J., Hyman, A.A., and Gerlich, D.W. (2016). Ki-67 acts as a biological surfactant to disperse mitotic chromosomes. Nature *535*, 308-312.

Faucher, D., and Wellinger, R.J. (2010). Methylated H3K4, a transcription-associated histone modification, is involved in the DNA damage response pathway. PLoS genetics *6*.

Folmes, C.D., Dzeja, P.P., Nelson, T.J., and Terzic, A. (2012). Metabolic plasticity in stem cell homeostasis and differentiation. Cell stem cell *11*, 596-606.

Gan, T., Jude, C.D., Zaffuto, K., and Ernst, P. (2010). Developmentally induced Mll1 loss reveals defects in postnatal haematopoiesis. Leukemia *24*, 1732-1741.

Gorospe, M., Wang, X., and Holbrook, N.J. (1999). Functional role of p21 during the cellular response to stress. Gene expression *7*, 377-385.

Gyori, B.M., Venkatachalam, G., Thiagarajan, P.S., Hsu, D., and Clement, M.V. (2014). OpenComet: an automated tool for comet assay image analysis. Redox biology *2*, 457-465.

Herbette, M., Mercier, M.G., Michal, F., Cluet, D., Burny, C., Yvert, G., Robert, V.J., and Palladino, F. (2017). The C. elegans SET-2/SET1 histone H3 Lys4 (H3K4) methyltransferase preserves genome stability in the germline. DNA repair *57*, 139-150.

Higgs, M.R., Sato, K., Reynolds, J.J., Begum, S., Bayley, R., Goula, A., Vernet, A., Paquin, K.L., Skalnik, D.G., Kobayashi, W.*, et al.* (2018). Histone Methylation by SETD1A Protects Nascent DNA through the Nucleosome Chaperone Activity of FANCD2. Molecular cell *71*, 25-41.e26.

Ito, K., Hirao, A., Arai, F., Matsuoka, S., Takubo, K., Hamaguchi, I., Nomiyama, K., Hosokawa, K., Sakurada, K., Nakagata, N.*, et al.* (2004). Regulation of oxidative stress by ATM is required for self-renewal of haematopoietic stem cells. Nature *431*, 997-1002.

Ito, K., and Suda, T. (2014). Metabolic requirements for the maintenance of self-renewing stem cells. Nature reviews. Molecular cell biology *15*, 243-256.

Jiang, H., Shukla, A., Wang, X., Chen, W.Y., Bernstein, B.E., and Roeder, R.G. (2011). Role for Dpy-30 in ES Cell-Fate Specification by Regulation of H3K4 Methylation within Bivalent Domains. Cell *144*, 513-525.

Kiel, M.J., Yilmaz, O.H., Iwashita, T., Yilmaz, O.H., Terhorst, C., and Morrison, S.J. (2005). SLAM family receptors distinguish hematopoietic stem and progenitor cells and reveal endothelial niches for stem cells. Cell *121*, 1109-1121.

Kohli, L., and Passegue, E. (2014). Surviving change: the metabolic journey of hematopoietic stem cells. Trends in cell biology *24*, 479-487.

Kondo, M., Wagers, A.J., Manz, M.G., Prohaska, S.S., Scherer, D.C., Beilhack, G.F., Shizuru, J.A., and Weissman, I.L. (2003). Biology of hematopoietic stem cells and progenitors: implications for clinical application. Annual review of immunology *21*, 759-806.

Kuhn, R., Schwenk, F., Aguet, M., and Rajewsky, K. (1995). Inducible gene targeting in mice. Science (New York, N.Y.) *269*, 1427-1429.

Li, T.S., and Marban, E. (2010). Physiological levels of reactive oxygen species are required to maintain genomic stability in stem cells. Stem cells (Dayton, Ohio) *28*, 1178-1185.

Lin, S.C., and Hardie, D.G. (2018). AMPK: Sensing Glucose as well as Cellular Energy Status. Cell metabolism *27*, 299-313.

Liu, J., Cao, L., Chen, J., Song, S., Lee, I.H., Quijano, C., Liu, H., Keyvanfar, K., Chen, H., Cao, L.Y.*, et al.* (2009). Bmi1 regulates mitochondrial function and the DNA damage response pathway. Nature *459*, 387-392.

Lukas, J., Lukas, C., and Bartek, J. (2011). More than just a focus: The chromatin response to DNA damage and its role in genome integrity maintenance. Nature cell biology *13*, 1161-1169.

Martin, C., and Zhang, Y. (2005). The diverse functions of histone lysine methylation. Nat Rev Mol Cell Biol *6*, 838-849.

Nijnik, A., Woodbine, L., Marchetti, C., Dawson, S., Lambe, T., Liu, C., Rodrigues, N.P., Crockford, T.L., Cabuy, E., Vindigni, A.*, et al.* (2007). DNA repair is limiting for haematopoietic stem cells during ageing. Nature *447*, 686-690.

Orkin, S.H., and Zon, L.I. (2008). Hematopoiesis: an evolving paradigm for stem cell biology. Cell *132*, 631-644.

Price, B.D., and D'Andrea, A.D. (2013). Chromatin remodeling at DNA double-strand breaks. Cell *152*, 1344-1354.

Rossi, D.J., Bryder, D., Seita, J., Nussenzweig, A., Hoeijmakers, J., and Weissman, I.L. (2007). Deficiencies in DNA damage repair limit the function of haematopoietic stem cells with age. Nature *447*, 725-729.

Santos, M.A., Faryabi, R.B., Ergen, A.V., Day, A.M., Malhowski, A., Canela, A., Onozawa, M., Lee, J.E., Callen, E., Gutierrez-Martinez, P.*, et al.* (2014). DNA-damage-induced differentiation of leukaemic cells as an anti-cancer barrier. Nature *514*, 107-111.

Scholzen, T., and Gerdes, J. (2000). The Ki-67 protein: from the known and the unknown. Journal of cellular physiology *182*, 311-322.

Shilatifard, A. (2008). Molecular implementation and physiological roles for histone H3 lysine 4 (H3K4) methylation. Curr Opin Cell Biol *20*, 341-348.

Simboeck, E., Gutierrez, A., Cozzuto, L., Beringer, M., Caizzi, L., Keyes, W.M., and Di Croce, L. (2013). DPY30 regulates pathways in cellular senescence through ID protein expression. The EMBO journal *32*, 2217-2230.

Stadtfeld, M., and Graf, T. (2005). Assessing the role of hematopoietic plasticity for endothelial and hepatocyte development by non-invasive lineage tracing. Development (Cambridge, England) *132*, 203-213.

Tasdogan, A., Kumar, S., Allies, G., Bausinger, J., Beckel, F., Hofemeister, H., Mulaw, M., Madan, V., Scharfetter-Kochanek, K., Feuring-Buske, M.*, et al.* (2016). DNA Damage-Induced HSPC Malfunction Depends on ROS Accumulation Downstream of IFN-1 Signaling and Bid Mobilization. Cell stem cell *19*, 752-767.

Viollet, B., Guigas, B., Leclerc, J., Hebrard, S., Lantier, L., Mounier, R., Andreelli, F., and Foretz, M. (2009). AMP-activated protein kinase in the regulation of hepatic energy metabolism: from physiology to therapeutic perspectives. Acta physiologica (Oxford, England) *196*, 81-98.

Yang, Z., Augustin, J., Chang, C., Hu, J., Shah, K., Chang, C.W., Townes, T., and Jiang, H. (2014). The DPY30 subunit in SET1/MLL complexes regulates the proliferation and differentiation of hematopoietic progenitor cells. Blood *124*, 2025-2033.

Yang, Z., Augustin, J., Hu, J., and Jiang, H. (2015). Physical Interactions and Functional Coordination between the Core Subunits of Set1/Mll Complexes and the Reprogramming Factors. PloS one *10*, e0145336.

Yang, Z., Shah, K., Busby, T., Giles, K., Khodadadi-Jamayran, A., Li, W., and Jiang, H. (2018). Hijacking a key chromatin modulator creates epigenetic vulnerability for MYC-driven cancer. The Journal of clinical investigation *128*, 3605-3618.

Yang, Z., Shah, K., Khodadadi-Jamayran, A., and Jiang, H. (2016). Dpy30 is critical for maintaining the identity and function of adult hematopoietic stem cells. The Journal of experimental medicine *213*, 2349-2364.

Yu, W.M., Liu, X., Shen, J., Jovanovic, O., Pohl, E.E., Gerson, S.L., Finkel, T., Broxmeyer, H.E., and Qu, C.K. (2013). Metabolic regulation by the mitochondrial phosphatase PTPMT1 is required for hematopoietic stem cell differentiation. Cell stem cell *12*, 62-74.

Zanella, A., Fermo, E., Bianchi, P., and Valentini, G. (2005). Red cell pyruvate kinase deficiency: molecular and clinical aspects. British journal of haematology *130*, 11-25.

Figure 1

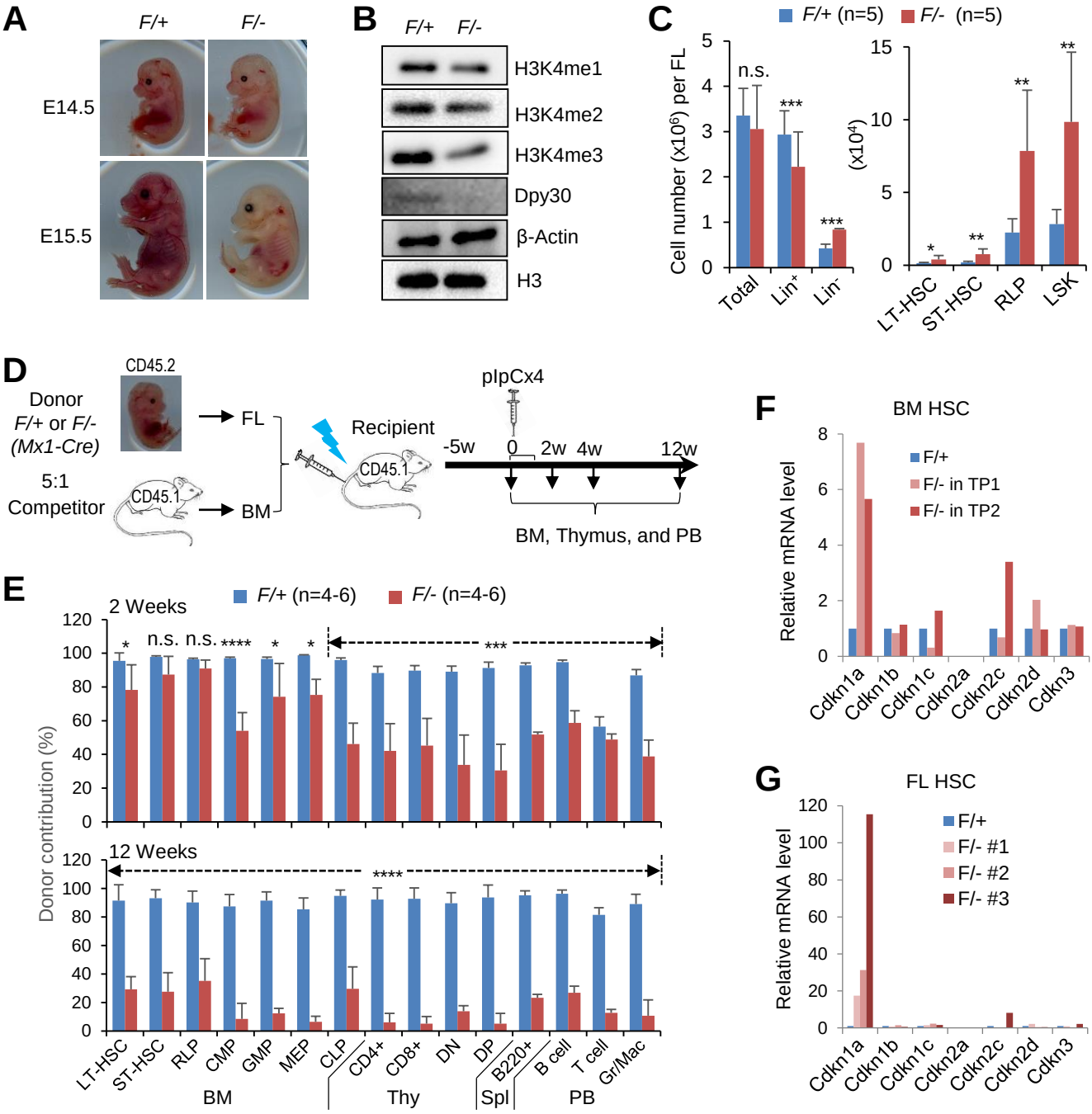
A
F/+
F/-
E14.5
E15.5
B
F/+
F/-
H3K4me1
H3K4me2
H3K4me3
Dpy30
β-Actin
H3
C
F/+ (n=5)
F/- (n=5)
Cell number (x10^6) per FL
n.s.
***
***
(x10^4)
*
**
**
**
Total
Lin+
Lin-
LT-HSC
ST-HSC
RLP
LSK
D
CD45.2
Donor
F/+ or F/-
(Mx1-Cre)
5:1
Competitor
CD45.1
FL
BM
Recipient
CD45.1
pIpCx4
-5w
0
2w
4w
12w
BM, Thymus, and PB
E
2 Weeks
F/+ (n=4-6)
F/- (n=4-6)
Donor contribution (%)
n.s.
n.s.
****
*
*
*
***
12 Weeks
****
LT-HSC
ST-HSC
RLP
CMP
GMP
MEP
CLP
CD4+
CD8+
DN
DP
B220+
B cell
T cell
Gr/Mac
BM
Thy
Spl
PB
F
BM HSC
Relative mRNA level
F/+
F/- in TP1
F/- in TP2
Cdkn1a
Cdkn1b
Cdkn1c
Cdkn2a
Cdkn2c
Cdkn2d
Cdkn3
G
FL HSC
Relative mRNA level
F/+
F/- #1
F/- #2
F/- #3
Cdkn1a
Cdkn1b
Cdkn1c
Cdkn2a
Cdkn2c
Cdkn2d
Cdkn3

Figure 2

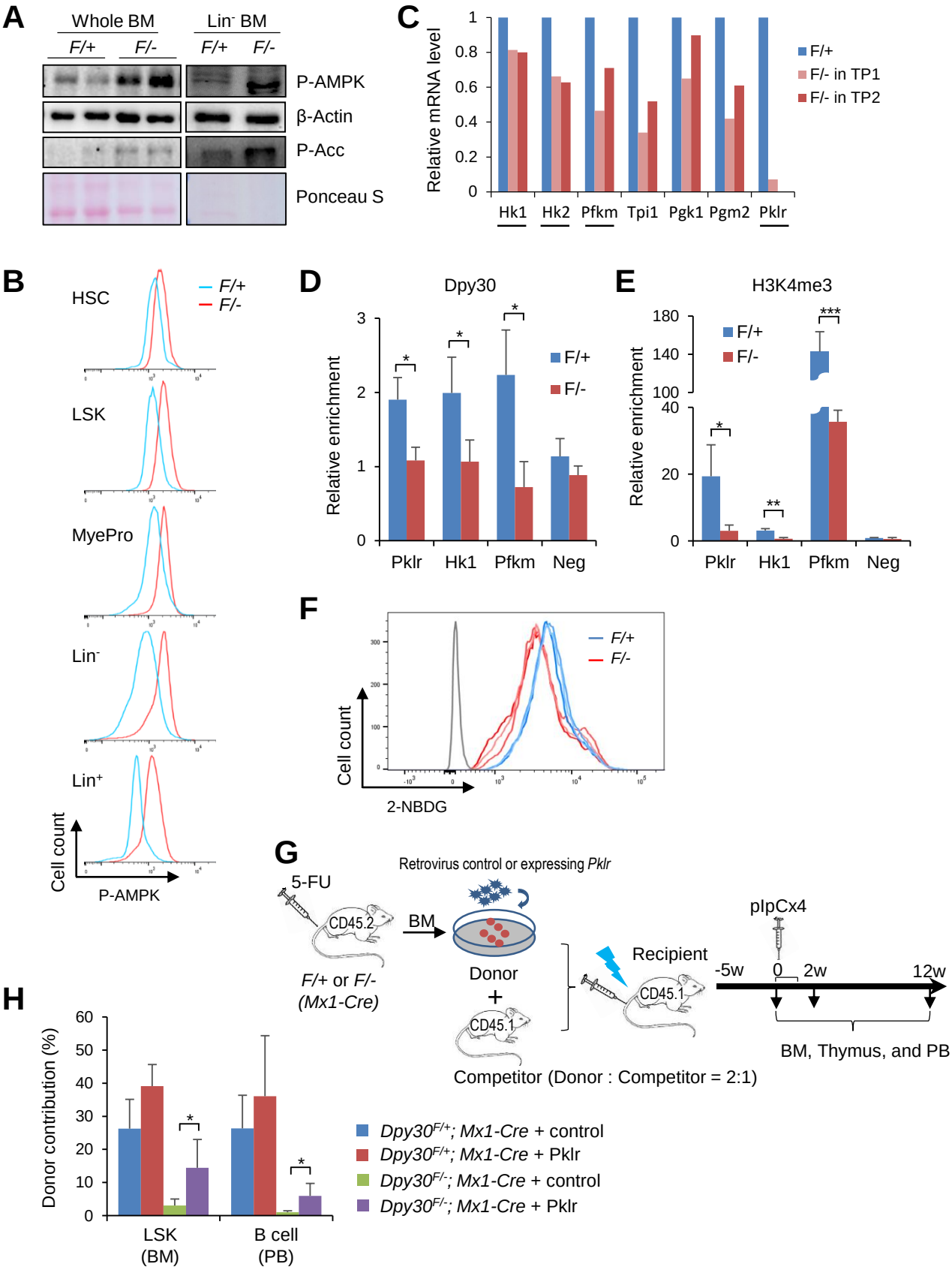
A
Whole BM
Lin- BM
F/+
F/-
F/+
F/-
P-AMPK
β-Actin
P-Acc
Ponceau S
C
Relative mRNA level
1
0.8
0.6
0.4
0.2
0
Hk1
Hk2
Pfkm
Tpi1
Pgk1
Pgm2
Pklr
F/+
F/- in TP1
F/- in TP2
B
HSC
LSK
MyePro
Lin-
Lin+
F/+
F/-
Cell count
P-AMPK
D
Dpy30
Relative enrichment
3
2
1
0
Pklr
Hk1
Pfkm
Neg
F/+
F/-
E
H3K4me3
Relative enrichment
180
140
100
40
20
0
Pklr
Hk1
Pfkm
Neg
F/+
F/-
F
Cell count
2-NBDG
F/+
F/-
G
5-FU
CD45.2
F/+ or F/-
(Mx1-Cre)
BM
Retrovirus control or expressing Pklr
Donor
+
CD45.1
Competitor (Donor : Competitor = 2:1)
Recipient
CD45.1
pIpCx4
-5w
0
2w
12w
BM, Thymus, and PB
H
Donor contribution (%)
60
50
40
30
20
10
0
LSK
(BM)
B cell
(PB)
Dpy30F/+; Mx1-Cre + control
Dpy30F/+; Mx1-Cre + Pklr
Dpy30F/-; Mx1-Cre + control
Dpy30F/-; Mx1-Cre + Pklr

Figure 3

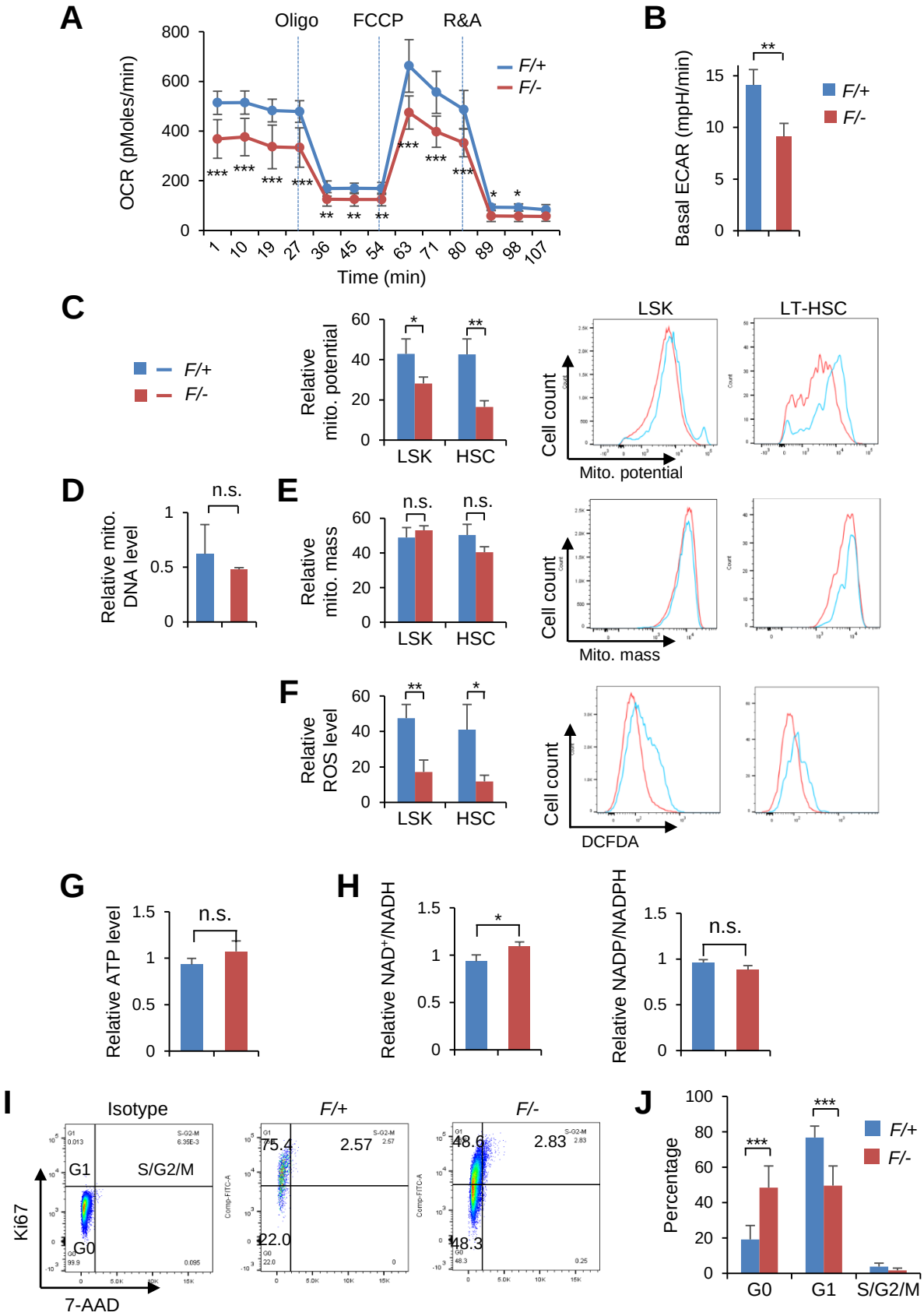
A
Oligo
FCCP
R&A
OCR (pMoles/min)
Time (min)
F/+
F/-
B
Basal ECAR (mpH/min)
C
Relative mito. potential
LSK
HSC
LT-HSC
Cell count
Mito. potential
D
Relative mito. DNA level
n.s.
E
Relative mito. mass
Mito. mass
F
Relative ROS level
DCFDA
G
Relative ATP level
H
Relative NAD+/NADH
Relative NADP/NADPH
I
Isotype
Ki67
7-AAD
G1
S/G2/M
G0
75.4
2.57
22.0
48.6
2.83
48.3
J
Percentage
G0
G1
S/G2/M

Figure 4

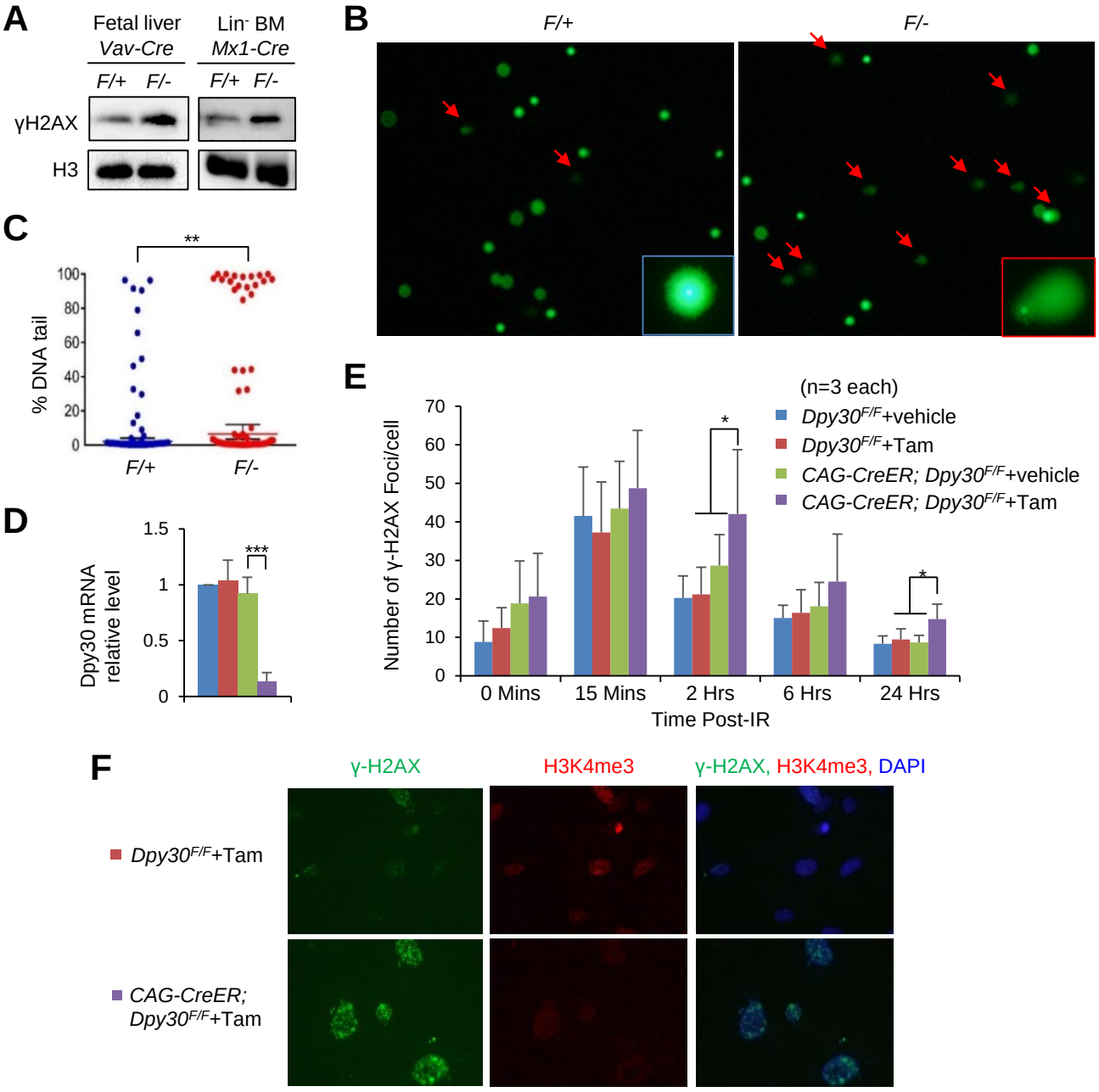
A
Fetal liver
Vav-Cre
Lin- BM
Mx1-Cre
F/+ F/-
F/+ F/-
γH2AX
H3
B
F/+
F/-
C
**
% DNA tail
100
80
60
40
20
0
F/+
F/-
D
Dpy30 mRNA relative level
1.5
1
0.5
0
***
E
(n=3 each)
Dpy30F/F+vehicle
Dpy30F/F+Tam
CAG-CreER; Dpy30F/F+vehicle
CAG-CreER; Dpy30F/F+Tam
Number of γ-H2AX Foci/cell
70
60
50
40
30
20
10
0
*
*
0 Mins
15 Mins
2 Hrs
6 Hrs
24 Hrs
Time Post-IR
F
γ-H2AX
H3K4me3
γ-H2AX, H3K4me3, DAPI
Dpy30F/F+Tam
CAG-CreER; Dpy30F/F+Tam

Figure 5

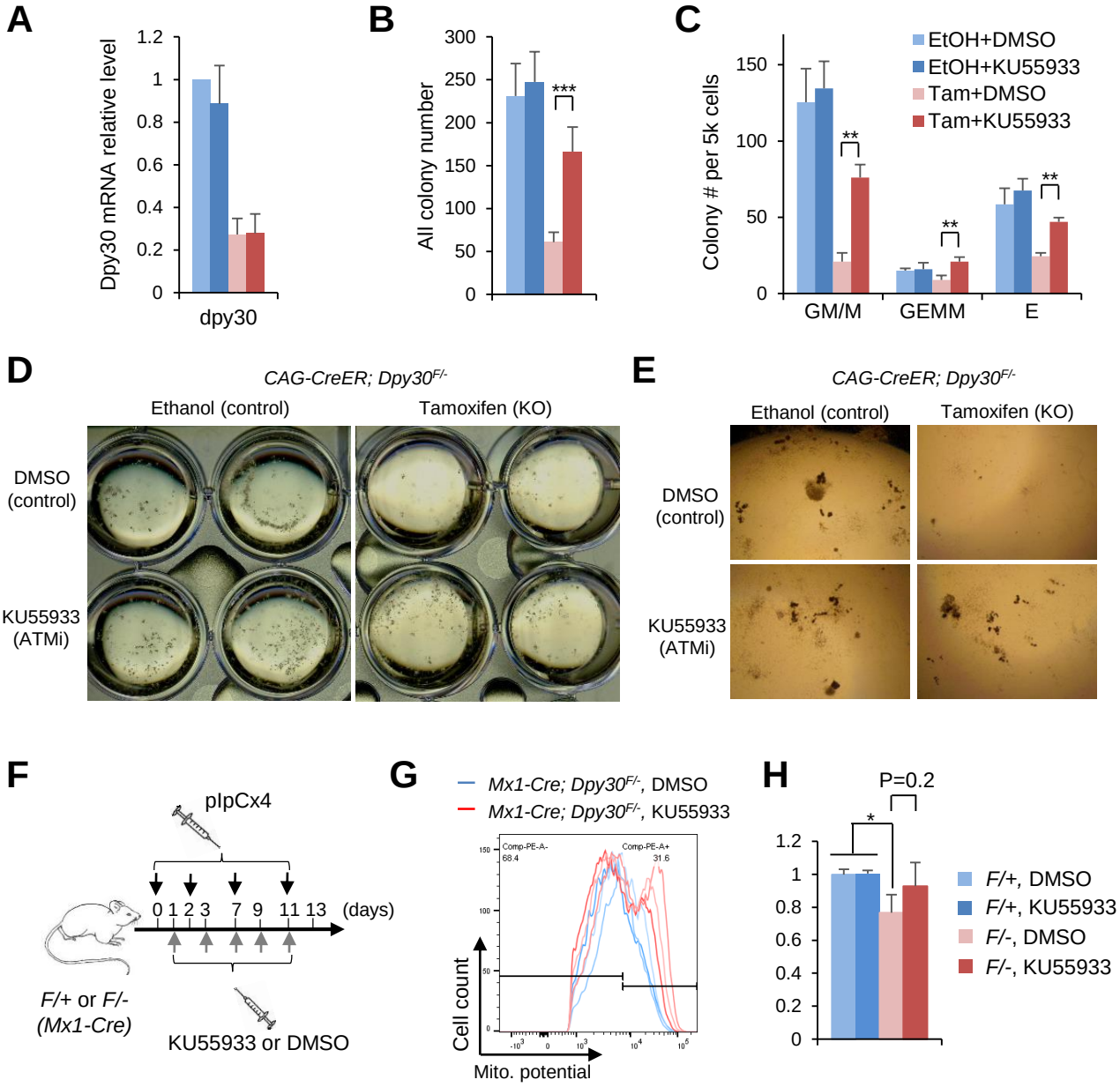
A
Dpy30 mRNA relative level
1.2
1
0.8
0.6
0.4
0.2
0
dpy30
B
All colony number
300
250
200
150
100
50
0
***
C
Colony # per 5k cells
150
100
50
0
**
**
**
GM/M
GEMM
E
EtOH+DMSO
EtOH+KU55933
Tam+DMSO
Tam+KU55933
D
CAG-CreER; Dpy30F/-
Ethanol (control)
Tamoxifen (KO)
DMSO (control)
KU55933 (ATMi)
E
CAG-CreER; Dpy30F/-
Ethanol (control)
Tamoxifen (KO)
DMSO (control)
KU55933 (ATMi)
F
pIpCx4
0 1 2 3 7 9 11 13 (days)
F/+ or F/- (Mx1-Cre)
KU55933 or DMSO
G
Mx1-Cre; Dpy30F/-, DMSO
Mx1-Cre; Dpy30F/-, KU55933
Comp-PE-A-
68.4
Comp-PE-A+
31.6
Cell count
Mito. potential
H
P=0.2
*
1.2
1
0.8
0.6
0.4
0.2
0
F/+, DMSO
F/+, KU55933
F/-, DMSO
F/-, KU55933

Figure 6

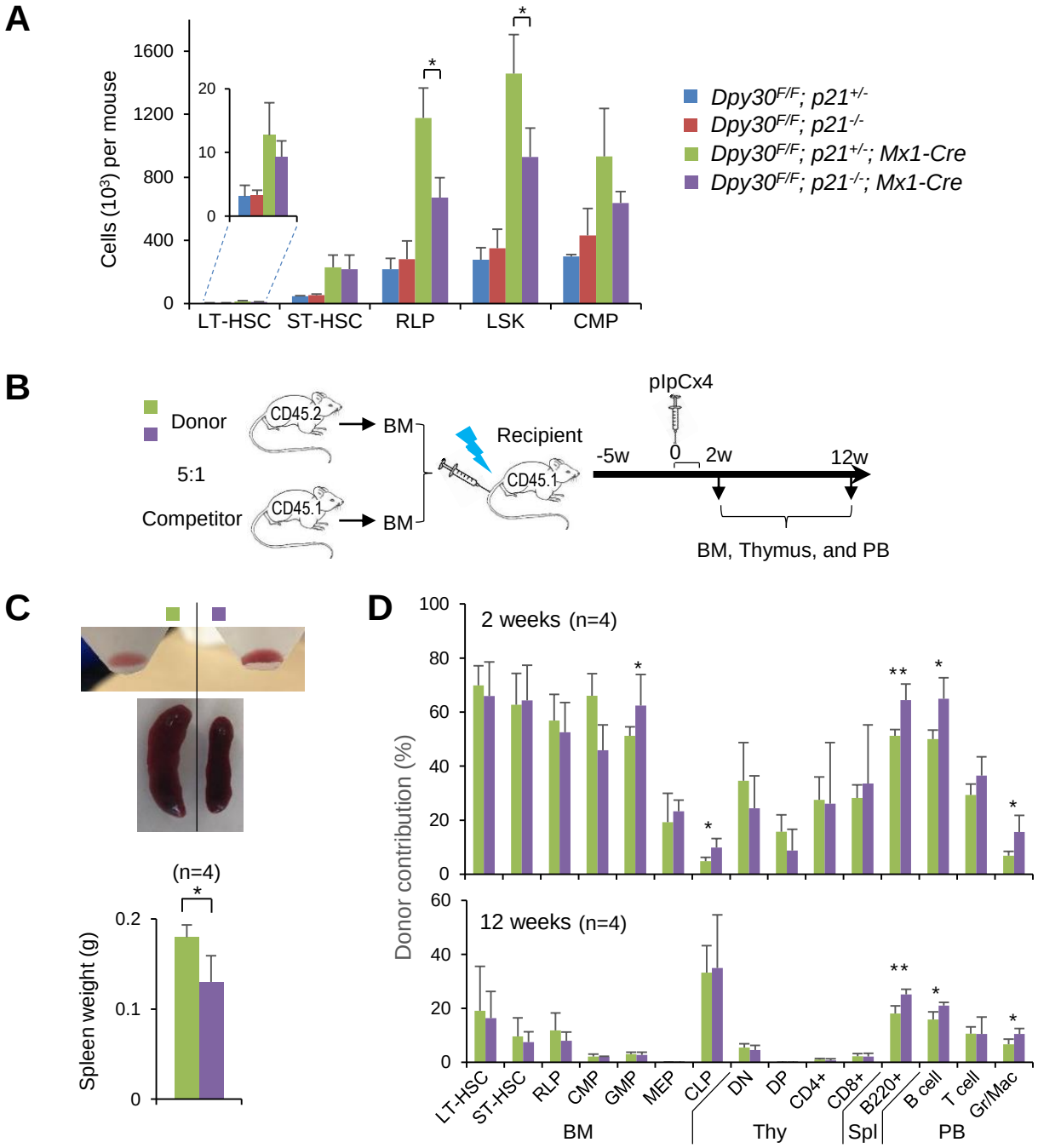
A
Cells (10^3) per mouse
1600
1200
800
400
0
20
10
0
*
*
LT-HSC
ST-HSC
RLP
LSK
CMP
Dpy30F/F; p21+/-
Dpy30F/F; p21-/-
Dpy30F/F; p21+/-; Mx1-Cre
Dpy30F/F; p21-/-; Mx1-Cre
B
Donor
5:1
Competitor
CD45.2
CD45.1
BM
BM
Recipient
CD45.1
pIpCx4
-5w
0
2w
12w
BM, Thymus, and PB
C
(n=4)
*
Spleen weight (g)
0.2
0.1
0
D
2 weeks (n=4)
12 weeks (n=4)
Donor contribution (%)
100
80
60
40
20
0
60
40
20
0
*
*
*
*
**
*
**
*
*
LT-HSC
ST-HSC
RLP
CMP
GMP
MEP
CLP
DN
DP
CD4+
CD8+
B220+
B cell
T cell
Gr/Mac
BM
Thy
Spl
PB

Figure 7

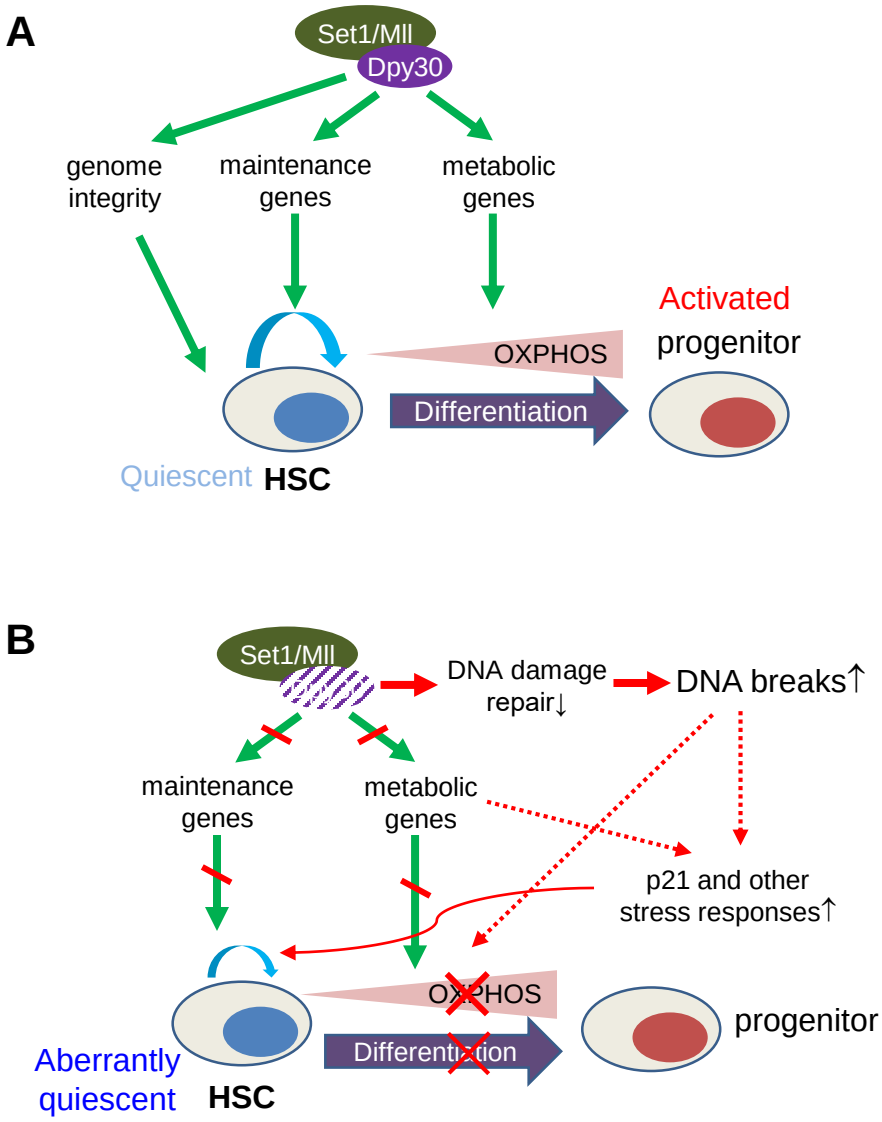
A
Set1/Mll
Dpy30
genome integrity
maintenance genes
metabolic genes
Activated
progenitor
OXPHOS
Differentiation
Quiescent HSC
B
Set1/Mll
DNA damage repair↓
DNA breaks↑
maintenance genes
metabolic genes
p21 and other stress responses↑
OXPHOS
Differentiation
progenitor
Aberrantly quiescent HSC

Supplemental Figure 1

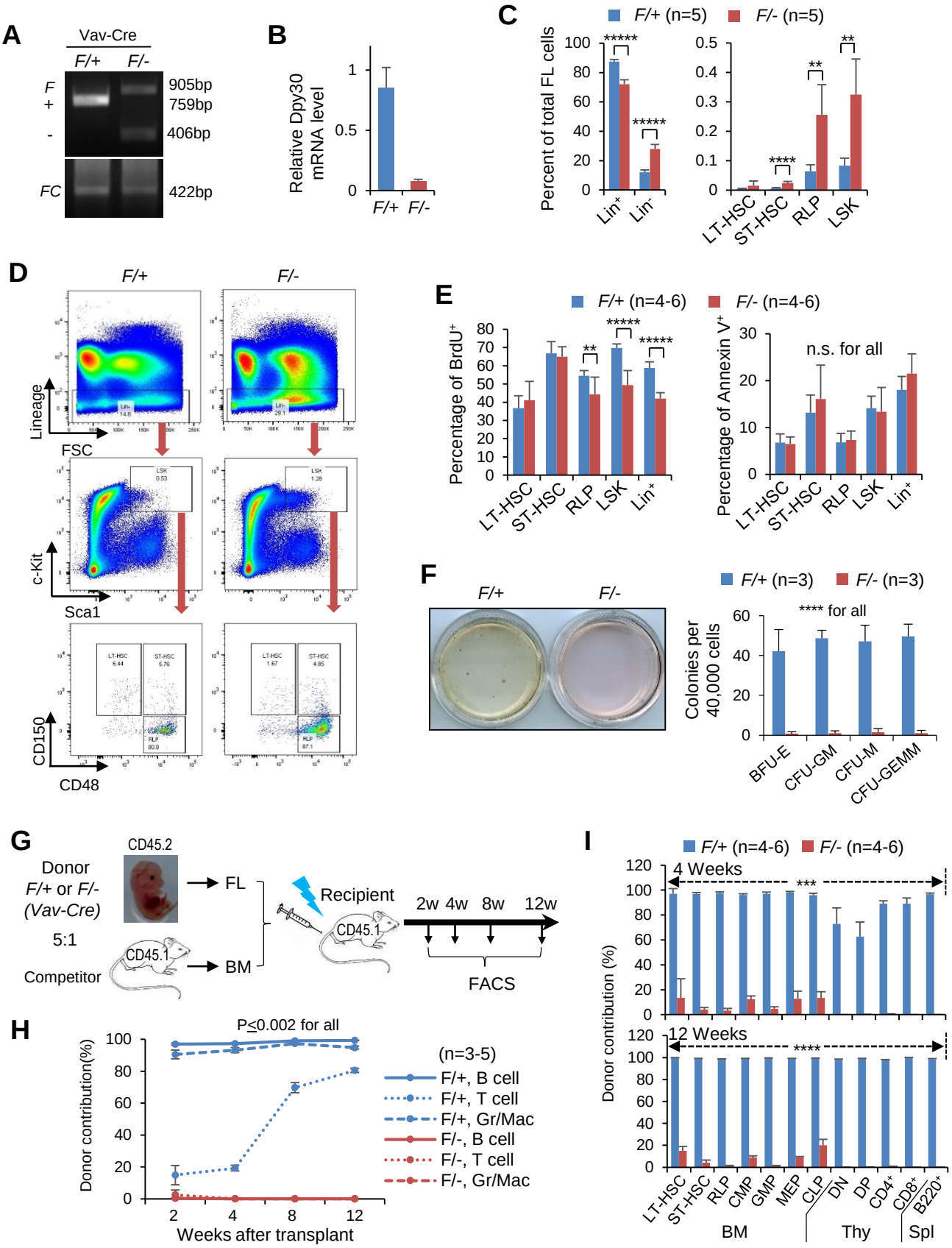

Supplemental Figure 2

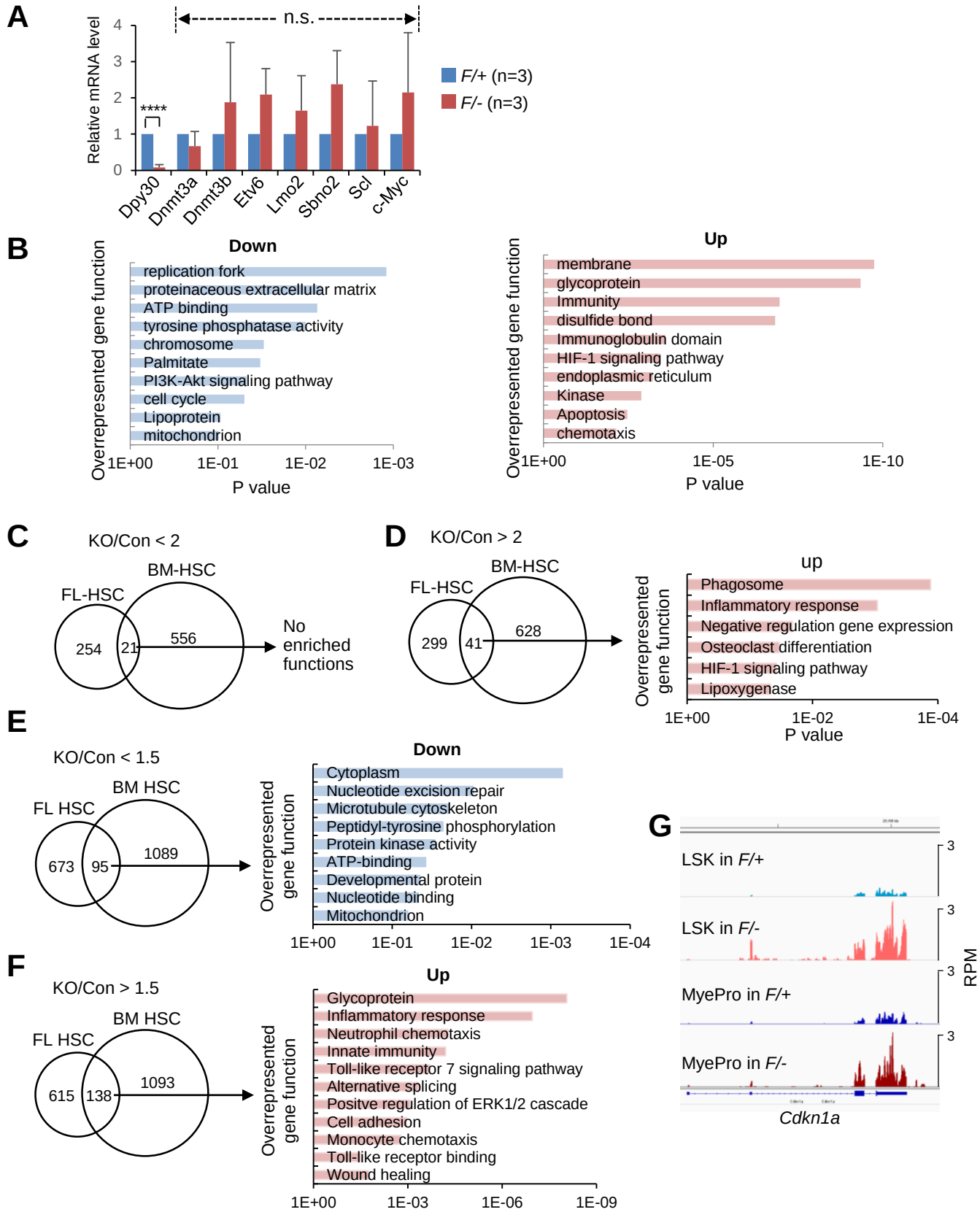

Supplemental Figure 3

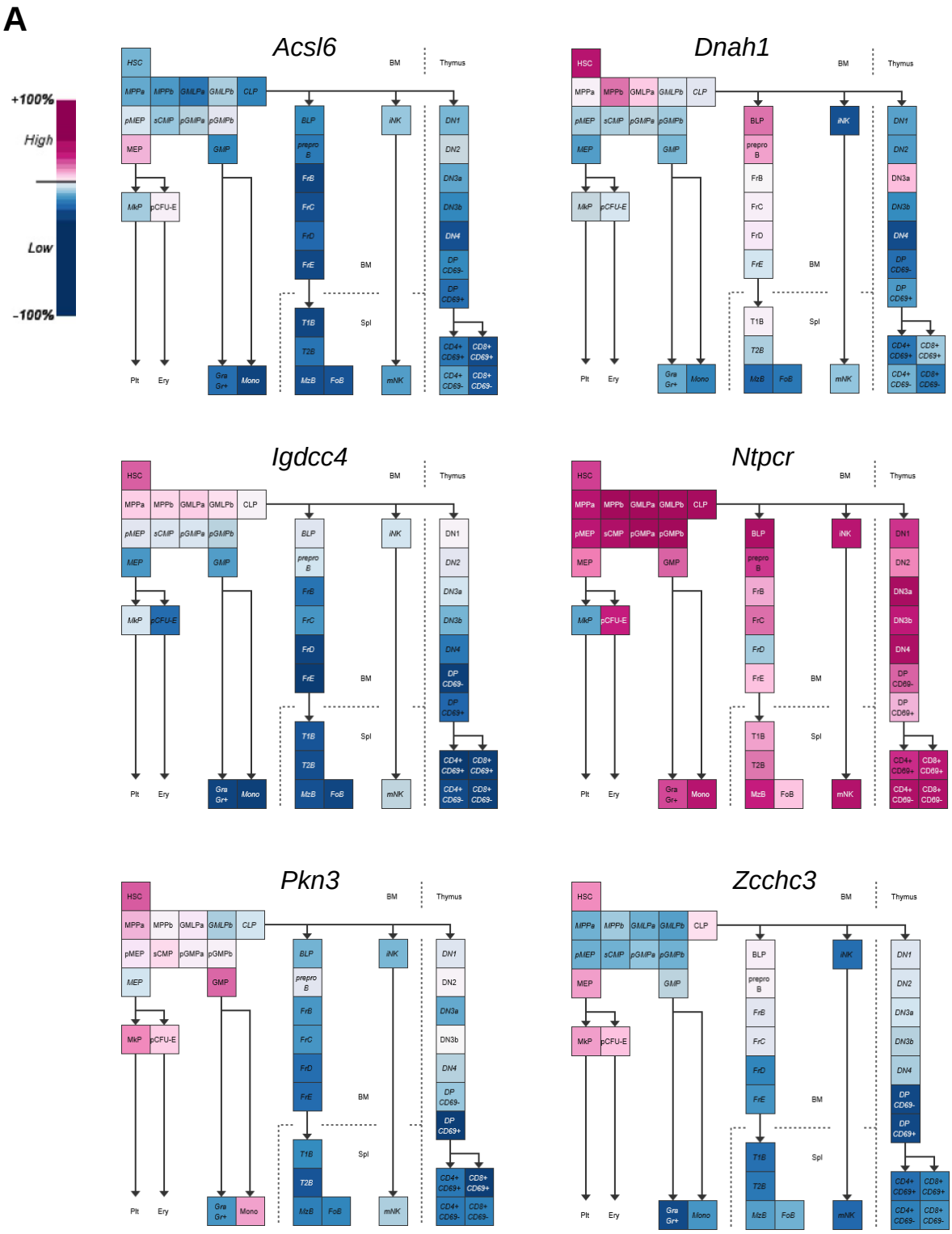

Supplemental Figure 3, continued

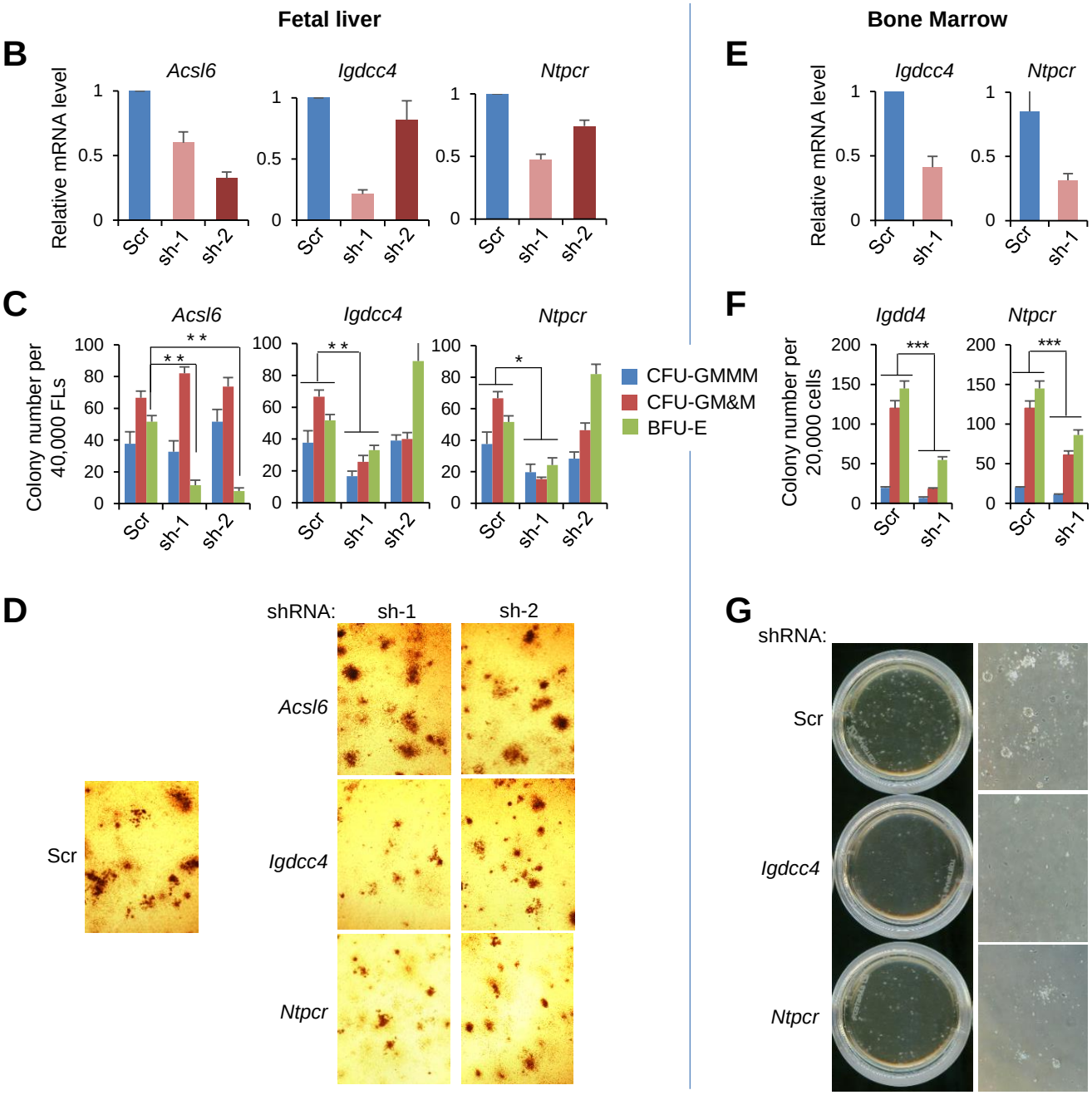

Supplemental Figure 4

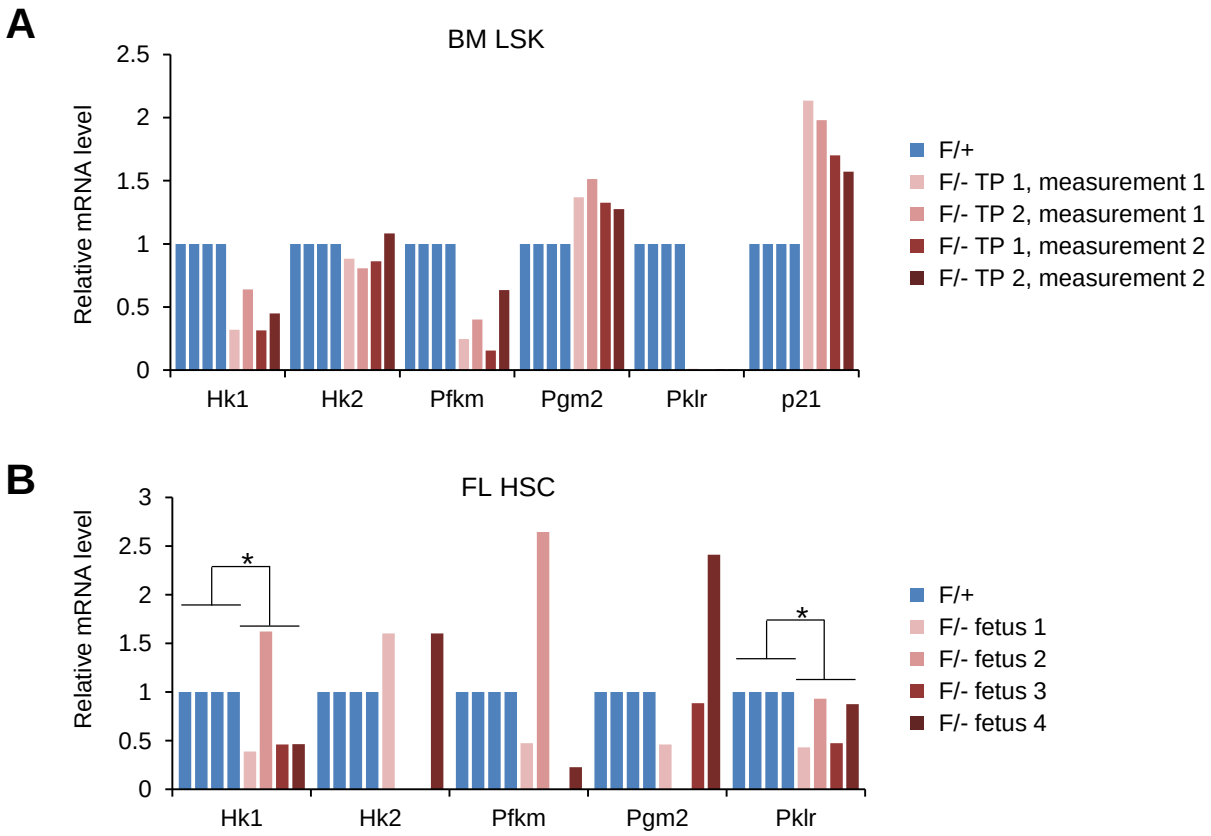

Supplemental Figure 5

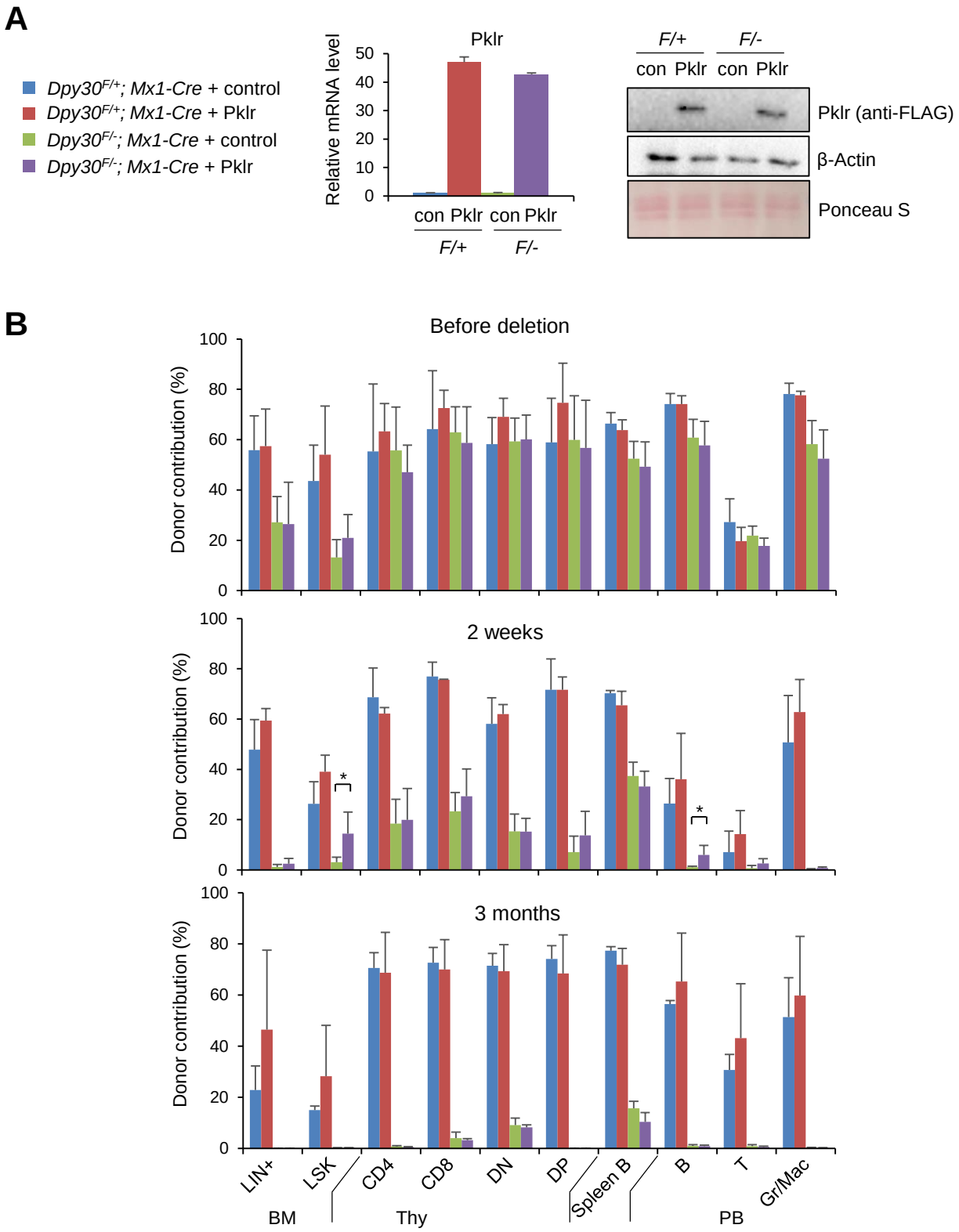

Supplemental Figure 6

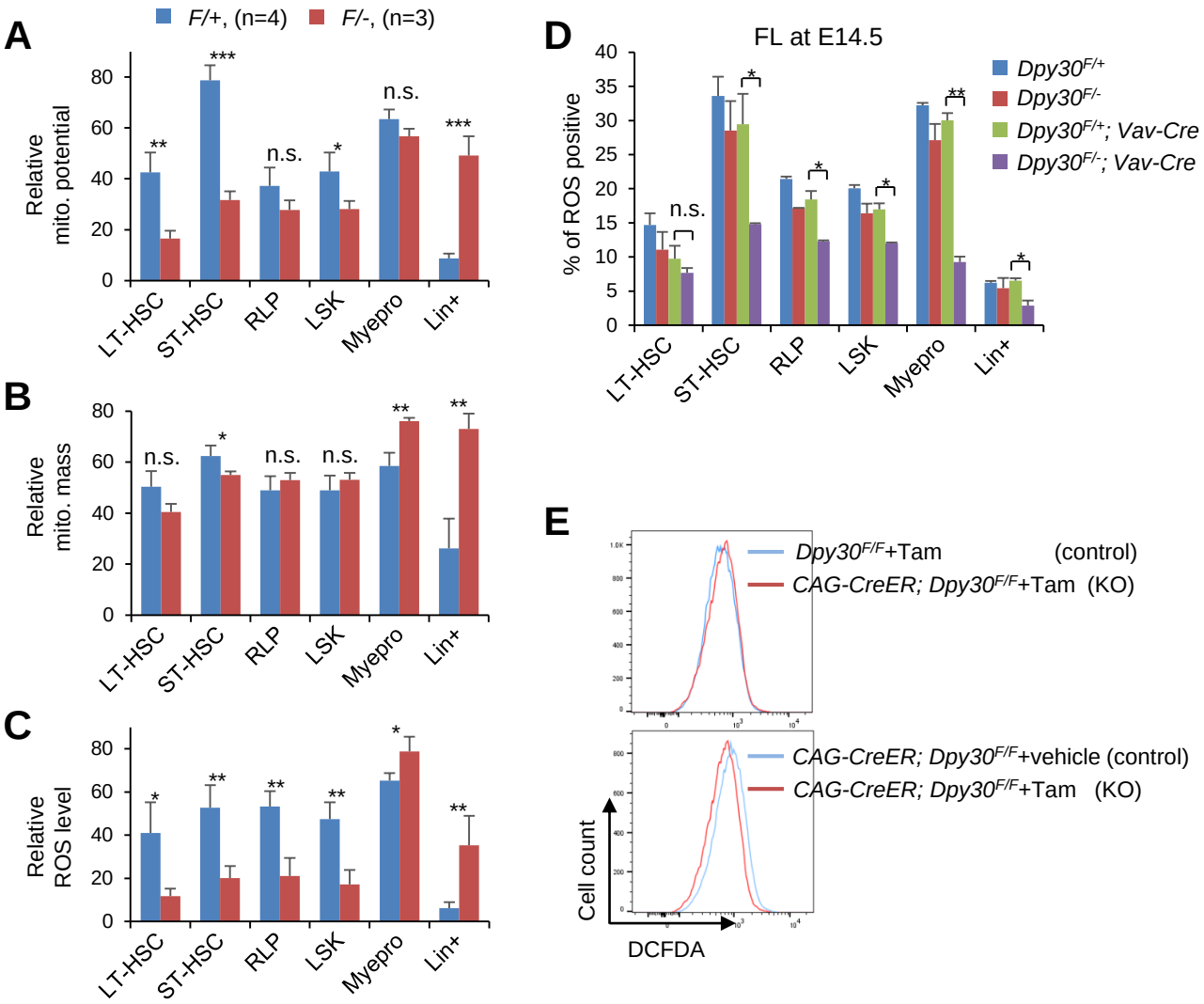
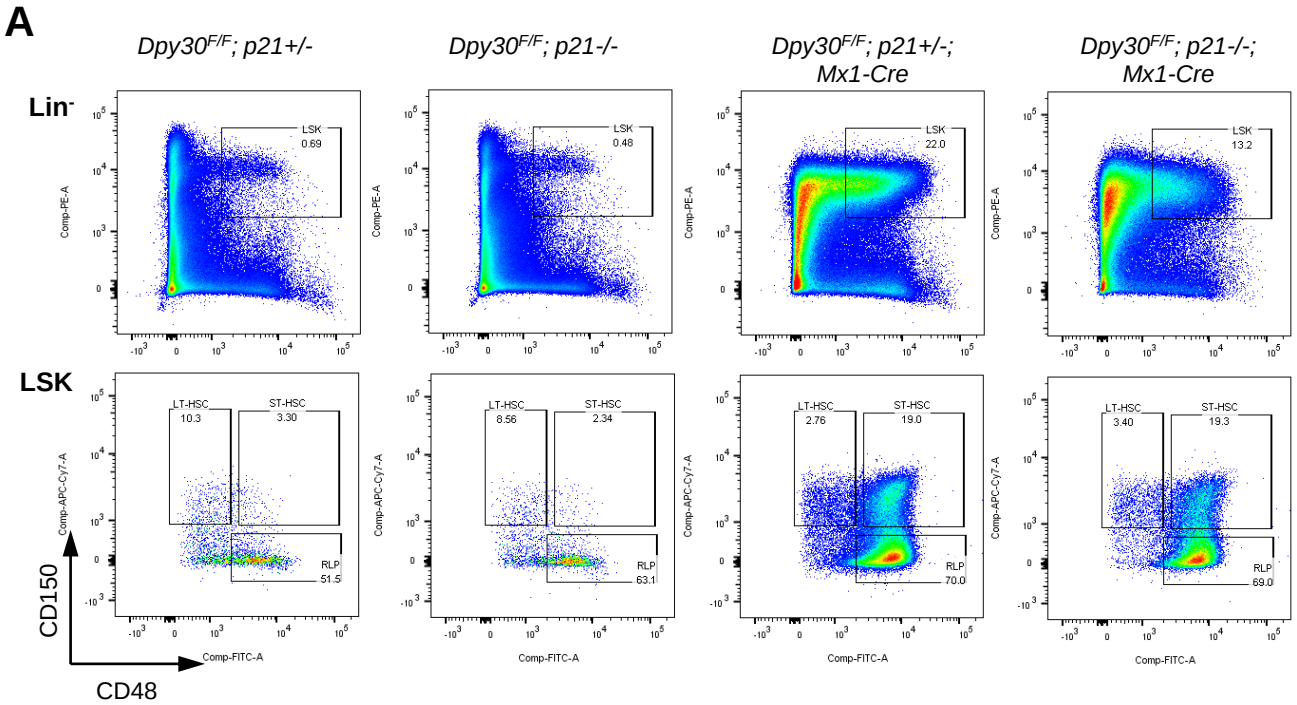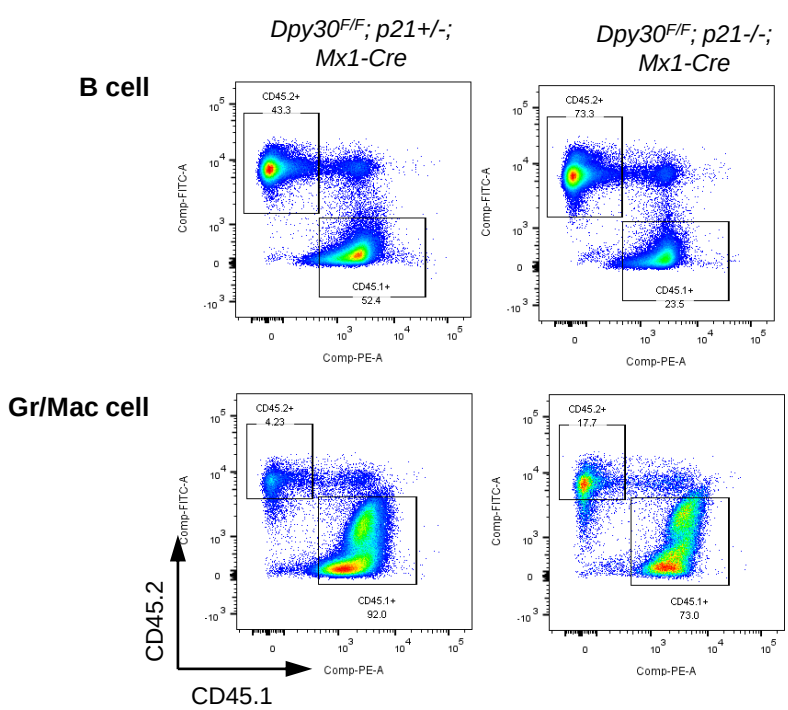
Supplemental Figure 7